

**TECHNISCHE
UNIVERSITÄT
DRESDEN**

Center for Molecular and Cellular Bioengineering (CMCB)

BIOTEC/CRTD

Master's program Nanobiophysics

**Quantification of cell interface dynamics
during mouse epiblast organoid formation
by using SPIM imaging and segmentation analysis**

A Thesis

By

Eric Schmidt

Submitted in partial fulfillment of the requirement

for the degree of
Master of Science

First Assessor: Prof. Alf Honigmann
Second Assessor: Dr. Robert Haase
Date of submission: 23.08.2022

Abstract

Stem-cell-based organoid model systems mimic different aspects of embryonic and organ development with a high level of control and accessibility. Furthermore, advances in microscopy techniques begin to shed light on single-cell behaviors that generate complex 3D tissues. With the generation of large microscopy data is the need for quantitative methods to segment and measure biological parameters in a robust manner.

In this thesis, I aimed to understand the process of lumenogenesis of mouse embryonic stem cells from a 3D geometrical perspective. This process occurs within maternal tissue and therefore has not been well-studied to date. To track the shapes and development of single cells and to simultaneously track the emerging lumen, I used 3D fluorescent cell culture, high-resolution time-lapse microscopy, and quantitative image analysis. Specifically, I developed a fully automated workflow to measure cell interface dynamics and apical receptor localization at the single cell level from 4D light-sheet microscopy data.

My work provides quantitative indicators for the transition from pluripotent stem cells to polarized epithelial cells by measuring the single cell production and localization of the apical membrane protein Podocalyxin (Podxl). By mapping the apical protein localization with respect to intercellular interfaces, I have shown that Podxl accumulates at higher order junctions over time. In the mouse epiblast, the lumen emerges in the center of a multicellular rosette, which is the area where all the cells meet. This suggests an essential role of geometrical self-organization for lumen formation in mouse embryonic stem cells. Furthermore, this quantitative analysis framework can be applied extensively to other 4D biological data to extract single cell interface dynamics for a better understanding of tissue formation processes.

Acknowledgments

Here I want to thank everyone who made it possible for me to finish my thesis.

First of all, I want to start with my supervisors who always found time in their tight schedules to discuss with me all topics of my thesis and who helped me with clear input, to find my own way. Thank you so much Prof. Alf Honigmann and Dr. Yara Alcheikh.

Thank you Prof. Alf Honigmann for accepting me into your wonderful lab. I am very happy about all the opportunities you gave me and about all the fruitful conversations we had. I could not be more thankful. It was a pleasure for me to work in your lab and I wish that we will continue working together in the future.

Thank you Dr. Yara Alcheikh for being always by my side when I needed someone to discuss the work. Thank you for all the conversations in and outside the lab. Thank you for providing me with tons of data and thank you for showing me all the techniques for running my own experiments.

Thank you to Dr. Robert Haase for being my second assessor and contact person for questions about image analysis. Thank you and all members of the Bio-image Analysis Group (PoL) for your support.

I also want to thank Dr. Karina Pombo-Garcia and Dr. Markus Mukenhirn for your biological input when I was showing you newly developed analysis tools. This always guided my work in a more biological relevant direction. Also, I want to thank all lab members for integrating me into the team very fast. It was a pleasure to spend my time in and outside the lab with you. Furthermore, I want to thank Manan Lalit for his introduction to the technical structures of the MPI. Thank you for being so motivating and open to everything.

Many thanks go to Deutschlandstipendium for providing me with financial support over the last year.

And last but not least, I want to thank my family and friends for always supporting me. Thank you for all the motivation and backup that you gave me. I am especially thankful to my girlfriend for going this way with me together and for listening to all my "interesting" stories about programming.

Finally, I want to thank my parents Kathleen and Andre Schmidt. Thank you for making it possible for me to grow up happily and without concerns about the future. Thank you for always believing in me when I wanted to pursue my passions.

Contents

Abstract	ii
Acknowledgments	iii
List of Tables	vii
List of Figures	ix
Acronyms	xi
1 Introduction	1
1.1 Morphogenesis	1
1.2 Mouse derived 3D epiblast organoids	4
1.3 High resolution microscopy	4
1.4 Data analysis	5
2 Aims	7
3 Materials and Methods	9
3.1 Preparation of mouse Embryonic Stem Cell (mESC) for organoid imaging	9
3.2 4D Spatiotemporal Imaging of mouse Embryonic Stem Cell (mESC) via Selective Plane Illumination Microscopy	9
3.3 Automated 3D instance segmentation, lineage tracing and 4D post-processing	10
3.3.1 3D instance-segmentation with PlantSeg	10
3.3.2 Segmentation artifact removal based on cell count and Connected Component Labeling (CCL)	13
3.3.3 Combine single classification errors with the most likely neighbor	15
3.3.4 Cell overlap calculation used as a measure for the segmentation accuracy and used for lineage tracing	17
3.3.5 Time information based post-processing to detect and remove segmentation errors	19

3.4	Data preparation for the quantification of single-cell parameters	21
3.4.1	3D Mesh reconstruction, Volume and Surface area measurement	21
3.4.2	Cell interface detection, classification, and analysis with respect to receptor and membrane concentration	22
3.4.3	Background subtraction in the Podocalyxin (Podxl) captures	24
3.4.4	Center of Mass based tracking of Podocalyxin	24
3.5	Quantification and statistical analysis	25
4	Results	27
4.1	3D Mouse epiblast organoids develop from single cells to organoids with lumen	27
4.2	Automated segmentation post-processing for improving accuracy and quantifying 4D segmented data is easier than ever before	28
4.3	mouse Embryonic Stem Cells (mESCs) proliferate and self-organize from a single cell to a 3D epiblast organoid with a single lumen	29
4.4	The pluripotent exit and the start of differentiation leads to a tremendous expression of Podocalyxin	31
4.5	Homogeneously distributed proteins are n-fold more concentrated in n-cellular junctions than in 1-cellular junctions	33
4.6	Non-homogeneously distributed apical receptor protein is higher concentrated in higher order junctions than in lower order junctions	35
4.7	Cells enrich Podocalyxin close to the geometrical center of the organoid, but still vary its exact position	37
5	Discussion	41
6	Conclusion	45
	Bibliography	47
	Declaration of Research Integrity and Good Scientific Practice	52

List of Tables

3.1 Model accuracy based on the Volume averaged Jaccard Index	12
3.2 Instance-segmentation algorithm accuracy based on the Volume averaged Jaccard Index.	13
3.3 Basic output structure of all performed measurements.	22
4.1 Descriptive statistics for the volume growth rate evaluation of Figure 4.2. .	30

List of Figures

1.1	Epiblast lumen formation in the egg cylinder and in the in vitro 3D culture.	2
1.2	Position and structure of Podocalyxin on the membrane and in the organoid.	3
1.3	Visualization of the principle of Selective Plane Illumination Microscopy.	5
3.1	Raw data and PlantSeg border prediction and instance segmentation.	11
3.2	Artifact removal after PlantSeg instance segmentation.	14
3.3	Merging of false classifications with real cells to obtain reasonable segmentation.	16
3.4	Lineage Tracing determined by the cell-cell overlap.	18
3.5	Watershed and time series based re-segmenting of wrong segmented, large, merged cells.	20
3.6	Algorithm for cell interface detection, classification and measuring for mono-, bi-, tri- and multi-cellular junctions	23
3.7	Segmentation-based background subtraction to filter out noise from the receptor captures.	24
4.1	The stages of mouse Embryonic Stem Cell development for membrane protein (CAAX) and Podocalyxin (Podxl) captures from single cells to organoid rosettes.	27
4.2	Cells within one organoid grow continuously with the same growth rate. . . .	30
4.3	The pluripotent exit of the cell is the starting point of tremendous receptor production.	32
4.4	The protein concentration increases step wise with the junction order. . . .	34
4.5	Non-homogeneously distributed Podocalyxin (Podxl) enriches in higher order junctions.	36
4.6	Podxl accumulates in the close distance around the geometrical Center of Mass (COM) of the organoid.	38

Acronyms

1J 1-cellular-junction

2J 2-cellular-junction

3J 3-cellular-junction

4J 4-cellular-junction

CAAX membrane protein

CCL Connected Component Labeling

CNN Convolutional Neural Network

COM Center of Mass

DL Deep Learning

GASP Generalized Algorithm for Signed graph Partitioning

GPU Graphics Processing Unit

GT Ground Truth

MDCK Madin-Darby Canine Kidney

mESC mouse Embryonic Stem Cell

ML Machine Learning

NG mNeonGreen

Podx1 Podocalyxin

SPIM Selective Plane Illumination Microscopy

VJI Volume averaged Jaccard Index

WS Watershed

1 Introduction

Single cells are the basic building blocks of complex tissues and organs that comprise an entire organism. In development, cells have to proliferate correctly, find the right position at the right time and differentiate to perform specific functions. The most fascinating aspect to my mind is that this process starts from one single cell, the fertilized egg.

A better understanding of tissue formation would bring uncountable advances in biological engineering and human health. It would lead to improved ways of constructing replacement organs for regenerative medicine and discovering the origin of developmental diseases and cancer.

1.1 Morphogenesis

Organs and tissues develop and form defined 3-dimensional shapes based on their biological functions, a process known as morphogenesis (Ducheyne, 2017). These shapes are controlled by the spatial distribution of the cells inside the tissue and the surrounding extracellular matrix.

The field of morphogenesis covers questions like: How are cell types arranged to get the final function? How are organs built up from tissues and how can these tissues build connections between each other? How does a cell know about its spatial location within a tissue or even within an organism? What stops a cell from growing in the wrong place? How do cells control their growth and how do they coordinate this with other cells? These and more questions can be found in books about developmental biology (Gilbert, 2001).

One important morphogenetic process during development is the creation of lumens in the center of connected cells called epithelia. Lumens are hollow spaces such as tubes present in mostly all internal organs such as kidneys and lungs and the early mammalian embryo (Sigurbjörnsdóttir, 2014).

Lumenogenesis

There are several mechanisms of lumen formation in developing tissues. One predominant mechanism is creating a lumen by the polarization of cells in the radial axis and the separation of the central contact point to create a lumen (Marciano, 2017). This can be seen for the mouse epiblast lumen in Figure 1.1.

This process has been studied extensively in Madin-Darby Canine Kidney (MDCK) cells, which are able to form 3D structures similar to kidney tubules when they are embedded as single cells in the extracellular matrix. From this model system, several protein players were discovered to have a key role in lumen formation. One of these

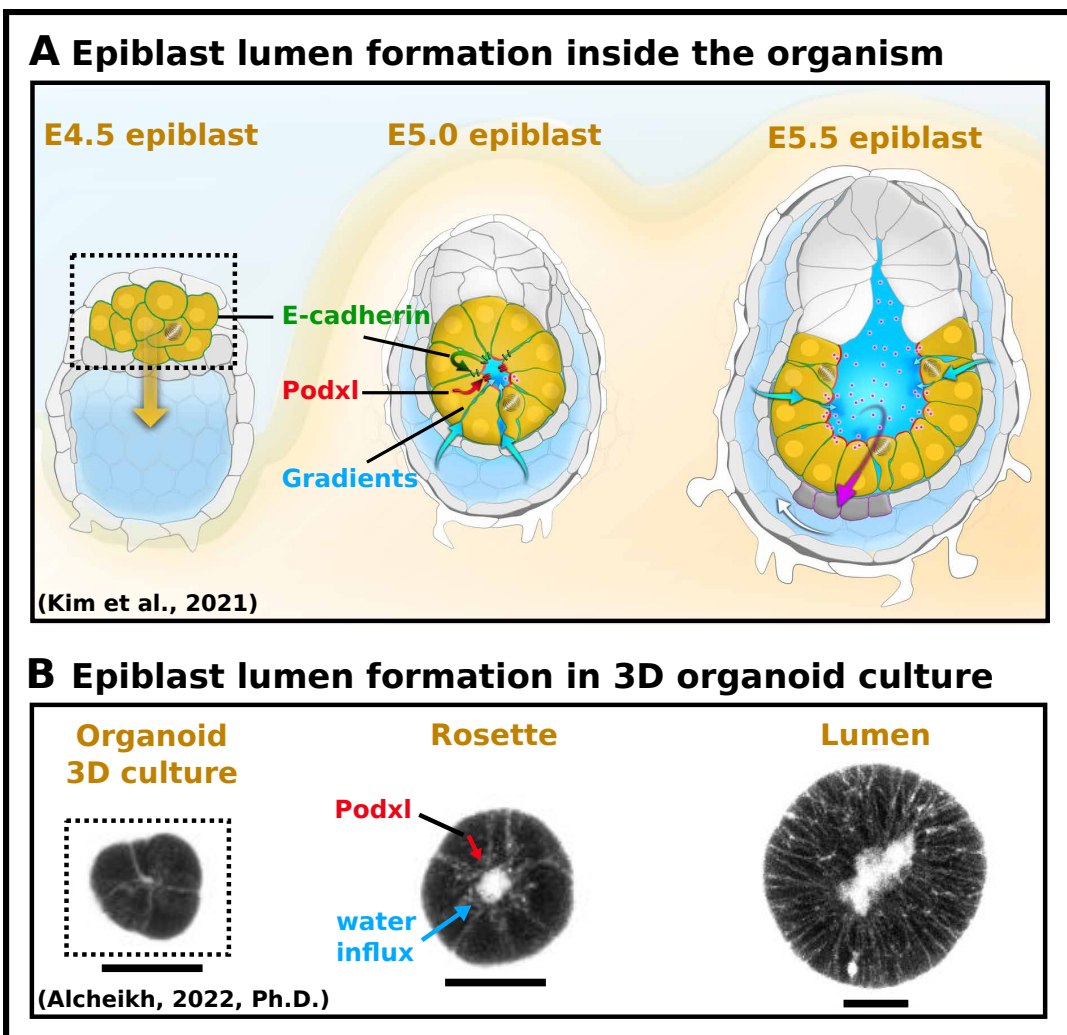


Figure 1.1: Epiblast lumen formation in the egg cylinder and in the in vitro 3D culture. A) Steps from the E4.5 epiblast to the E5.5 epiblast under influence of E-Cadherin, Podocalyxin (Podxl) and water and ion gradients. Adapted from (Kim, 2021)¹. B) In vitro 3D epiblast organoid development from E4.5 state to rosette and lumen state, imaged with dextran (white) entering the cell. The expression of Podocalyxin (Podxl) proteins is from highest interest in this thesis. Adapted from (Alcheikh, 2022). The scale bar is 20 μ m.

proteins is a membrane-connected receptor protein called Podocalyxin (Podxl). This receptor is anti-adhesive, and negatively charged and it is the first important protein for building up the lumen surface by building the apical plasma membrane (Bryant 2010; Ferrari 2008). The structure and position of Podxl is shown in Figure 1.2. First, Podxl is present homogeneously along the membrane of single cells. Upon the first cell division, the receptor is taken up internally and transported in vesicles towards the center of the dividing cell. There, Podxl leaves the cytoplasmic vesicular pool and fuses to the membrane to create a new apical membrane.

¹©Yung Su Kim (CC BY 4.0), adapted by: Eric Schmidt

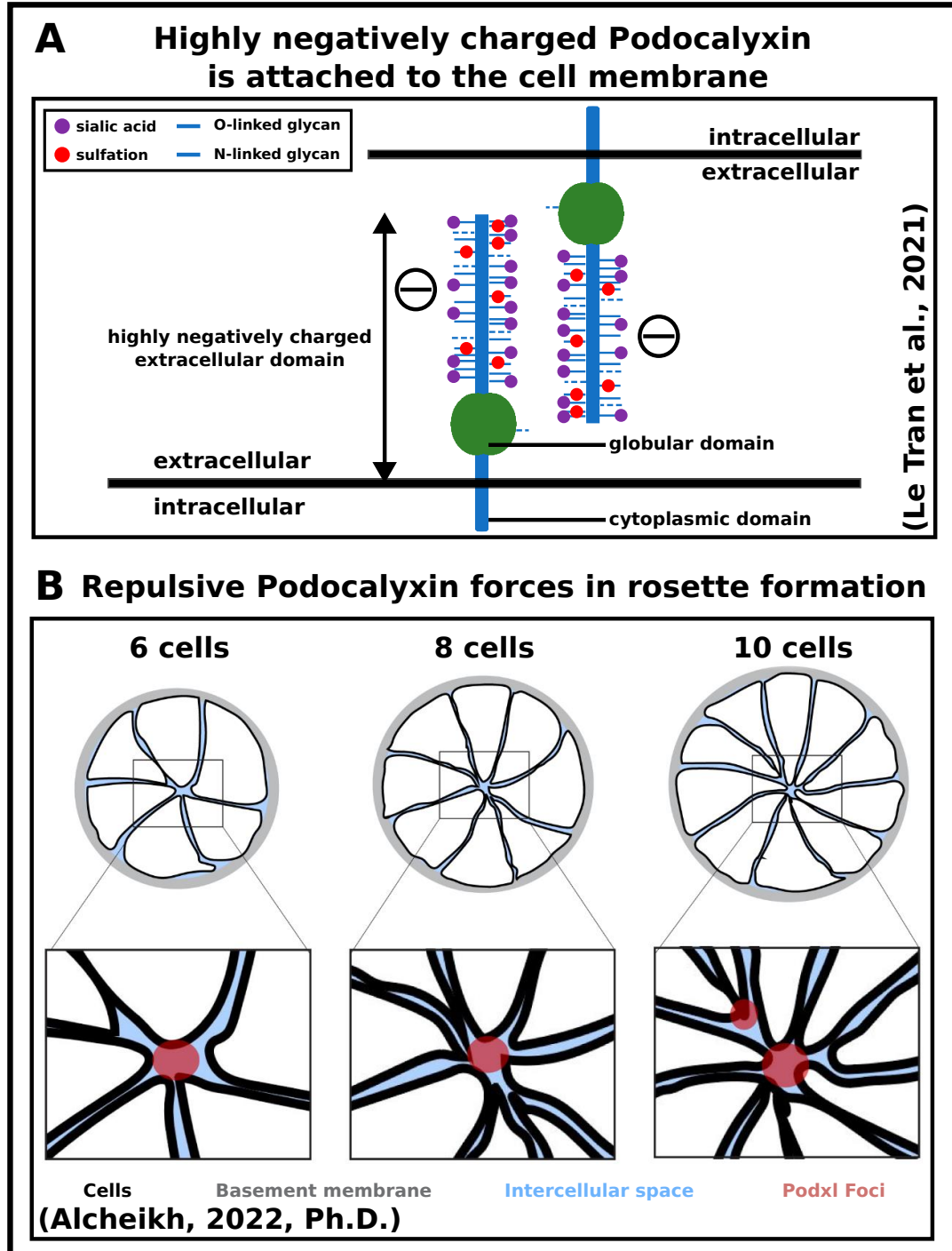


Figure 1.2: [Position and structure of Podocalyxin on the membrane and in the organoid. A) Glycosylated and negatively charged Podxl is attached to the membrane and repulsive to other negatively charged proteins. Adapted from (Le Tran, 2021; McNagny, 2012)². B) Podxl accumulation in the organoid during rosette formation. Adapted from (Alcheikh, 2022).

²©Kelly M. McNagny, Michael R. Hughes and Ngoc Le Tran (CC BY 4.0), adapted by: Eric Schmidt

A lumen is then created by the separation of the opposing cell membranes by electrostatic repulsion of Podxl and it expands by the influx of water driven by the establishment of ion pumps and osmosis. Therefore in MDCK apical polarization after the first cell division directly leads to lumen formation (Bryant, 2014; Klinkert, 2016).

1.2 Mouse derived 3D epiblast organoids

These findings are valid for already differentiated kidney cells which have all the polarization components already expressed, but how a lumen is generated from pluripotent stem cells is not well understood. For this, our lab is using stem cells derived from the E4.5 blastocyst mouse embryo. mouse Embryonic Stem Cell (mESC) have the advantage of being genetically similar to the human, develops fast, and are able to self-organize to structures similar to what they do in the organism.

With inhibitor-based protocols (Smith, 1988; Williams, 1988) it is nowadays possible to keep the embryonic stem cells in a pluripotent cell state by inhibiting cell differentiation. Once the pluripotent cells are then seeded in an extracellular matrix (Matrigel) in media without inhibitors, they start differentiating to create 3D cultures, called organoids. In our protocol (Martin-Lemaitre, 2020), mESC loses its pluripotency and differentiates to form an epiblast epithelium with a central lumen when embedded as single cells in Matrigel, similar to the mouse and human embryos during implantation. The epiblast is the structure that gives rise to all the cells of the organism.

These 3D organoids are relatively small (10-50 μm) and thus are optically accessible. To be able to visualize both the shapes of the cells as well the creation of the lumen, mESCs have been genetically modified to have fluorophores attached to the membrane protein (CAAX) which is a membrane domain and to the apical receptor protein Podxl which specifically labels the apical membrane. The fluorophores are mNeonGreen (NG) and mScarlet respectively. In order to observe in real time the formation of epiblast organoids with a central lumen, we need to be able to image with high resolution in time and space without harm to the cells. For this, Selective Plane Illumination Microscopy (SPIM) is the method of choice.

1.3 High resolution microscopy

Imaging fluorescent cells in real-time and with high signal-to-noise for quantitative single-cell analysis is challenging. This is due to cell phototoxicity and bleaching of the fluorophores from laser exposure. These problems are prevalent in high-resolution imaging such as confocal microscopy which generates out-of-focus light in the entire axial plane, which causes phototoxicity and bleaching. In recent years, SPIM has revolutionized developmental cell biology by enabling long-term imaging of cells for highly

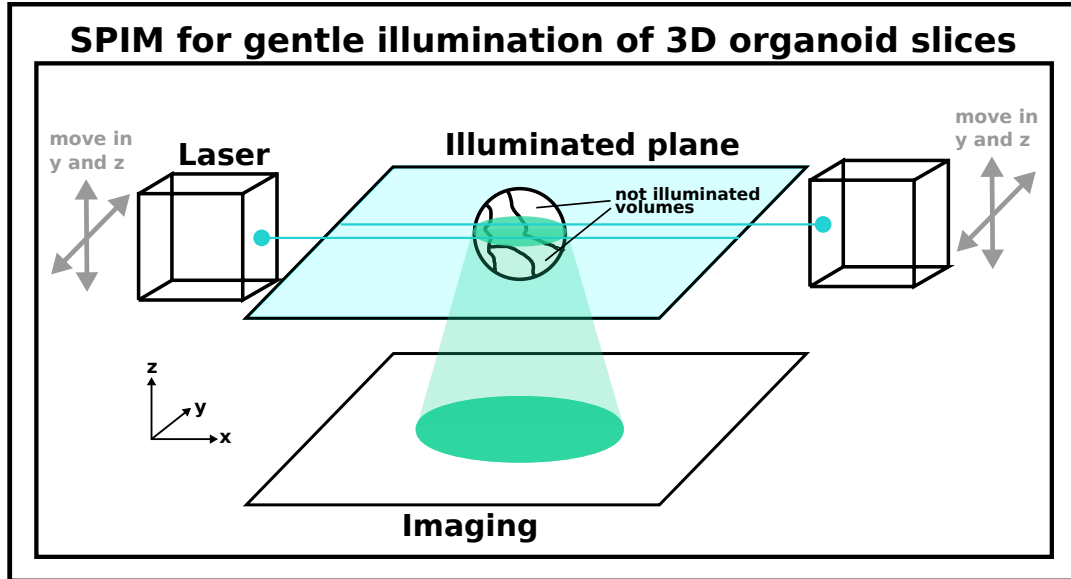


Figure 1.3: Visualization of the principle of Selective Plane Illumination Microscopy. Two lasers which are parallel shifted, illuminate the xy plane, in which the organoid is. Moving the lasers fast in y direction, illuminates the plane. Moving the laser in z, illuminates another z-slice. Not illuminated volumes are above and below the illuminated plane. The imaging happens with a camera.

quantitative multidimensional analysis (Huisken, 2004). The general setup for SPIM is shown in Figure 1.3. The organoid is inside a matrigel and two lasers are focused on it. These lasers are slightly parallel shifted (in y and in z) so that the resulting beam(s) are homogeneous (with a less dominant beam waist). Then, both lasers are moved fast in the y direction to illuminate the complete plane of the organoid. After taking an image of the fluorescence, lasers are lifted in z.

Although the spatial resolution is generally lower compared to confocal imaging, it is still an excellent resolution for the segmentation of the signal. Furthermore, it maximizes cell survival by exciting only in the z-plane being imaged and thus also minimizes bleaching of the fluorescent signal. We use a custom organoid SPIM which is equipped with 5 % CO₂ and 37 °C which mimic the cell culture growth conditions and equipped with a specialized imaging chamber where the cells are easily mounted for imaging.

1.4 Data analysis

Once the spatiotemporal videos are acquired, a tremendous amount of data has to be analyzed. The quantitative analysis was one of the bottlenecks in 4D systems, due to a large amount of data. In the last years, computer scientists put a lot of effort into the automatized, quantitative, objective, and reliable analysis of images. This effort lead

to handy tools like ImageJ³ (Schindelin, 2012) or Napari⁴ (Sofroniew, 2022). With the offspring of Machine Learning (ML), Deep Learning (DL) and Graphics Processing Unit (GPU)-accelerated processing, this toolbox was extended by applications like Cellpose⁵ (Stringer, 2020), StarDist⁶ (Schmidt, 2018), EmbedSeg⁷ (Lalit, 2022), and PlantSeg⁸ (Wolny, 2020). All these tools make it possible to segment big data sets, which was not feasible before.

Unfortunately, a computer does not reach the accuracy of an expert, so there is still a lot of human post-processing necessary to clean up the predictions of the machine. To tackle this issue, I aimed to automatize the post-processing step by making it fast, easy to use, objective and reliable. This allows to segment big amounts of data in a short time and to perform single cell-based quantification.

³ImageJ GitHub: <https://github.com/imagej/ImageJ>, 21.08.2022

⁴Napari GitHub: <https://github.com/napari/napari/tree/v0.4.16>, 21.08.2022

⁵Cellpose GitHub: <https://github.com/MouseLand/cellpose>, 21.08.2022

⁶StarDist GitHub: <https://github.com/stardist/stardist>, 21.08.2022

⁷EmbedSeg GitHub: <https://github.com/juglab/EmbedSeg>, 21.08.2022

⁸PlantSeg GitHub: <https://github.com/hci-unihd/plant-seg>, 21.08.2022

2 Aims

To study morphological changes during the early mouse epiblast organoid formation in 3D over time, it is necessary to have optically accessible cells. These cells have to cover the time span from the single cell state, up to the state of early lumen formation and beyond. The aim is to image these cells in all these stadiums to study morphology in a three-dimensional system to compare with and extend the result from two-dimensional studies. This thesis covers 4 main topics. The first two topics are (i) morphogenesis studies of mESCs during embryonic development and (ii) the study of receptor expression dependent on the state of embryonic development. Topic (iii) is to quantify the accumulation of protein along the cell interfaces for all cell cycles. To fulfill these aims, the main work of this thesis was the development of a python based analysis pipeline, which performs automated post-processing of 3D segmentations. This pipeline brings the data into an easily accessible structure for quantification analysis.

Building up an automated quantitative analysis framework

We ultimately aim to understand the geometrical process of lumen formation of mouse embryonic stem cells in 3D at the single cell level together with the protein polarization which results in the emergence central apical lumen. With the tools at hand, such as robust cell culture methods for growing epiblast organoids, fluorescent cell lines for two-color imaging with both cell shapes and apical membrane protein, and SPIM which enables imaging over several days with high resolution, I aimed to build a quantitative analysis framework to extract single cell information about the geometry and protein distribution which are required for lumenogenesis.

(i) Do mouse embryonic stem cells change the volume and surface growing rate based on the cell cycle?

Working with mESCs is a rarely discovered and especially rarely quantified field at the moment. Morphological processes, like the proliferation of cells, are widely studied and understood for other model organisms, but not yet for 3D mESC organoids. It is the aim to use single cell-based tracking to quantify morphological properties like the volume (cytoplasm) and surface area (membrane) growth rate during the development of the cells. These studies are important for understanding the influence of the cell cycle, cell neighborhood, volume, nutrient supply, etc. on the growth of a single cell.

(ii) Do cells produce membrane proteins depending on the cell cycle with a feedback system or do they produce these proteins permanently?

From cell and lumen development studies, it is shown that cells need to produce membrane receptors (especially Podxl) to drive the process of lumen formation during embryonic development (Bryant 2014). For this, cells produce the membrane receptors

and use either vesicular transport or diffusion to relocate the receptors. It is known from these studies that lumen formation would not work properly without these receptors (Doyonnas, 2001).

It is now the aim to quantify, if the cell can actively control the production of the receptor depending on the situation (development time, neighbor cells, etc.) or if the cell is passively, permanently producing the same amount of receptor until the lumen forms.

(iii) Does apical receptor accumulate preferably in higher ordered junctions and does this leads to rosette formation and lumen opening?

From previous development studies, it is known that embryonic single cells grow, reshape and reorganize to a rosette formation, which then opens a further growing cavity (Bedzhov, 2014). Interestingly, this process happens naturally in all lumen building mESCs and it is still not clear why. Within this thesis, I want to quantify, how expressed apical receptor is split up between different kinds of junctions. This can solidify knowledge from MDCK studies or open new interpretation possibilities. In general, the study here is important, to understand lumenogenesis.

3 Materials and Methods

3.1 Preparation of mESC for organoid imaging

To analyze the cell interface dynamics in 4D, the mESCs are prepared, following the protocol of Andrea Meinhardt (Meinhardt, 2014) and Cécilie Martin-Lemaitre (Martin-Lemaitre, 2020) and imaged with a Viventis SPIM microscope.

For this, the organoids have to grow in N2B27 differentiation medium, which has to be, as well as the enzyme accutase, pre-warmed to 37 °C in the first step. Thawing the Matrigel on ice at the same time. Usage of a 40 µm cell strainer helps to filter out dead, not agglomerated cells, which were growing in pluripotency media (2i/Lif). Invert the filter and flush the agglomerated cells with 1-2 mL of accutase from the filter into a 10 cm dish. Incubate the cells with accutase for 2 min at 37 °C and pipette them afterward 5 times gently up and down to activate the enzyme and assure contact with the cells. After this, incubate again for 2 min at 37 °C. Then add 8 mL of N2B27 differentiation medium and pipette 6-10 times up and down against the glass wall to split up the last aggregated cells. These cells are now in a differentiation medium.

Now check for single cells under the light microscope and remove aggregates via filtration through a 40 µm cell strainer. Transfer the suspension in a 15 mL tube and centrifuge at 800 rcf for 3 min to separate the cells from accutase. Discard the supernatant afterward and snip with the finger against the tube wall to loosen the cell pellet. Add 3-8 mL of differentiation medium to the pellet and mix everything by pipetting the cells up and down. Count the cells with a counting chamber (hemocytometer).

Now re-suspend the cells in a 1 mL Eppendorf tube in 100 % Matrigel at the ratio of 300 cells/µL of Matrigel. Prepare at least 5 µL of cell-Matrigel to fill one Viventis multi-well chamber of the SPIM microscope. Finally, prepare the microscope chambers by filling the Viventis multi-well chambers with 5 µL of cell-Matrigel each and incubating them at 37 °C for 20 minutes. Add after incubation, 200 µL of N2B27 media to every chamber and continue incubating overnight before starting imaging.

3.2 4D Spatiotemporal Imaging of mESC via Selective Plane Illumination Microscopy

After preparing the cells with overnight incubation, one can start imaging the cell-Matrigel Viventis chambers under culturing conditions. For this, prepare the microscopy chamber of the SPIM microscope with 5 % CO₂ concentration (body conditions), 37 °C, and a water bath for keeping constant humidity. Load the sample, close everything and start imaging with bright field microscopy to search for the cells. Magnification of 1.5x is sufficient.

Use the software to align both lasers globally and locally for every cell of interest to perform SPIM microscopy. Set the optical density to 2 or 3 depending on the Signal-to-Noise ratio and the light sensitivity of the cells. Set all regions of interest as (x,y,z)-range. Enable tracking of the cells if the absolute velocity information of the cells is not needed. Set the delay between two 3D scans to 10 minutes. Set the laser wavelengths and exposure times to 488 nm, 50 ms for the membrane imaging (NG-tagged CAAX) and to 561 nm, 50 ms for the (mScarlet-tagged) Podxl imaging. Set a beam thickness of $2.2 \mu\text{m}$.

Set the save directory and start the measurement for all positions. Run the measurement until the cells start to die. Cells that die start to lose brightness in the membrane channel, because the fluorophore is not expressed anymore.

Living cells express all fluorophores properly and can be analyzed automatically by using DL algorithms and post-processing.

3.3 Automated 3D instance segmentation, lineage tracing and 4D post-processing

Analyzing mESCs in 4D to quantify cell interface dynamics means here, analyzing several videos consisting of over 100 time steps, with a stack size of approximately 50 z-slices (with $1 \mu\text{m}$ per slice), which ends up in over 5 000 images. The field of instance-segmentation is made for the task of labeling every instance (here: individual cells) in an image.

To analyze the spatial data, the open-source, deep learning-based tool PlantSeg (Wolny, 2020) is used. PlantSeg offers several prediction models, but all of them lead to artifacts by using them on the here acquired data. Hence it is necessary to remove artifacts, fix errors, and validate the results. Additionally, for temporal analysis, it is necessary to connect the predictions from one time step with the predictions for another time step. The time connection information can then be used to fix errors. Finally the (in ideal case) error-free segmentation can then be used for data quantification and also for training the DL model again.

All these steps (besides training of the DL network) are described in the following parts, beginning with the instance-segmentation tool PlantSeg.

3.3.1 3D instance-segmentation with PlantSeg

PlantSeg is a DL based tool for 3D-instance segmentation, which performs essentially two steps. The first step is to predict a probability map for boundaries and the second step is to fill these predictions with a graph partitioning algorithm with labels to obtain

the final segmentation. The usage of PlantSeg is described in the PlantSeg GitHub⁹ and in the corresponding paper (Wolny, 2020). PlantSeg is used for the mESC data

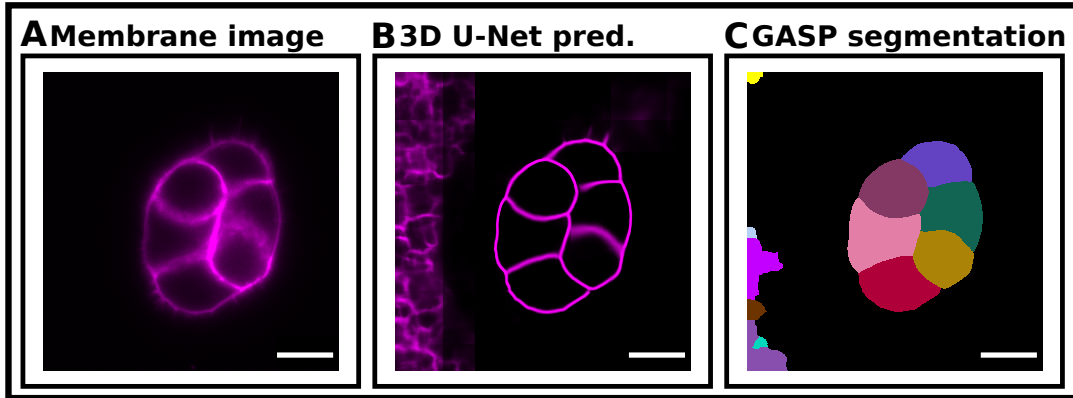


Figure 3.1: Raw data and PlantSeg border prediction and instance segmentation. A) SPIM image of the cell membrane for $t,z = \text{const.}$ B) PlantSeg's integrated 3D U-Net predicts the probability for a pixel to be in the foreground of the slice. Bright pixels are classified as foreground, whereas dark pixels belong to the background. C) The Generalized Algorithm for Signed graph Partitioning (GASP) segmentation performs the final instance-segmentation. PlantSeg introduces artifacts along the image border. The scale bar is $10 \mu\text{m}$.

because it consists of a U-Net-based architecture (Ronneberger, 2015), which is adapted to 3D (Cicek, 2016) and state of the art in predicting borders of volumetric images.

⁹PlantSeg GitHub: <https://github.com/wolny/pytorch-3dunet/>

Secondly, because PlantSeg has the Generalized Algorithm for Signed graph Partitioning (GASP) (Bailoni, 2019) and other graph partitioning algorithms for the final segmentation implemented. These are again state of the art segmentation algorithms (compare with Figure 3.1).

3D U-Net settings

To obtain the 3D U-Net results ("Convolutional Neural Network (CNN) prediction") of Figure 3.1 B, PlantSeg needs the "model name" as input, which is here the pre-trained "generic_light_sheet_3d_unet" model. Additionally, it needs the "patch" size, "stride" size, and "mirror padding" size as input. To perform the predictions GPU-accelerated, the "device" has to be set to "cuda". For this, it needs a cuda capable GPU.

Patch and stride sizes have to be adapted to fit into the GPU memory. The patch size refers to the size of a matrix (a "kernel"), which is used to scan over the 3D capture and is the visible volume for the 3D U-Net for this step. The stride size is the size, for which the patch will be shifted in the following step. With that, the stride size defines the overlap between two patches. A large overlap (a small stride size) leads to a smooth prediction map in the 3D U-Net prediction (compare Figure 3.1 B), but also to more steps and longer run times.

For a GPU with 4 GB memory and an image dimension of $(z, y, x) = (54, 299, 296)$ px, a patch size of $(54, 128, 128)$ and a stride size of $(16, 64, 64)$ is a sufficient compromise between accuracy, speed and GPU memory.

The generic light sheet 3D model is chosen because it performs better than all other pre-trained models. The performance test was done by testing the prediction results against a Ground Truth (GT) with the Volume averaged Jaccard Index (VJI) as a measure. A VJI close to 1 is perfect. A description of the calculation of the VJI comes in section 3.3.4). The results for two MultiCut instance-segmentations, compared with the GT time steps are shown in Table 3.3.

Table 3.1: Model accuracy based on the Volume averaged Jaccard Index.

The GT consists of two time steps, which are manually annotated. The VJI is defined in section 3.3.4 and ranges from 0 (no overlap) to 1 (perfect overlap).

GT	generic light sheet 3d unet	mouse embryo confocal model	confocal unet bce dice ds3x	confocal PNAS 3d
T = 0 min + 24 h	0.786	0.220	0.755	0.764
T = 60min + 24 h	0.898	0.144	0.848	0.866

Instance Segmentation settings

For the second step of instance segmentation, PlantSeg offers four algorithms. The al-

gorithms are MultiCut, MutexWS, GASP, and DtWatershed. By testing the prediction results against a GT with the VJI as a measure, it turned out that MultiCut, MutexWS, and GASP perform equally good after using the generic light sheet 3D U-Net model. Only DtWatershed could not handle the 3D U-Net predictions. The results are in Table 3.2 and the description of the VJI follows in section 3.3.4.

Due to the fact that the best performer from these two measurements (MultiCut) ended up in infinity loops for certain time steps, it is a good choice to use GASP as the segmentation algorithm (second best performance).

Table 3.2: Instance-segmentation algorithm accuracy based on the Volume averaged Jaccard Index.. The GT consists of two time steps, which are manually annotated. The VJI is defined in section 3.3.4 and ranges from 0 (no overlap) to 1 (perfect overlap).

GT	DtWatershed	MultiCut	GASP	MutexWS
T = 0 min + 24 h	0.090	0.786	0.787	0.784
T = 0 min + 24 h	0.110	0.898	0.896	0.894

The instance-segmentation needs parameter fine tuning to reach the best results. The parameters with the highest impact are the "beta" value and the "Watershed (WS) threshold". The parameter "beta", as described in the PlantSeg paper (Wolny, 2020) tunes the over- and under-segmentation. The parameter "WS threshold" tunes the number of seeds. The other parameters can stay untouched. The "WS 2D" option has to be set to "False", to use 3D information for the segmentation.

Even the best settings for the GASP instance segmentation can not help to remove the artifacts, which arise from the 3D U-Net predictions. To handle these artifacts, network re-training with an ideal GT or post-processing is necessary.

3.3.2 Segmentation artifact removal based on cell count and Connected Component Labeling (CCL)

PlantSeg introduces artifacts into the predictions. They have to be removed. The artifact removed captures can then be used to re-train the network (not done in this thesis). The artifacts for this kind of data can be seen in Figure 3.1 C or in Figure 3.2. These artifacts are characterized by the properties:

- 1) small objects in x-y plane compared to the real cells
- 2) small objects in z expansion compared to the real cells
- 3) not touching the organoid
- 4) sometimes touching the image border.

Hence, post-processing is here a reduction to the problem of creating a mask for the organoid and deleting everything else. One important tool for telling the computer the

difference between objects is CCL. CCL uses binary images (images with only 2 values, mostly 0 and 1) as input and identifies the non-background pixels with a certain class (labeling). Before the label is given to a pixel, the algorithm combines neighbor pixels together, so that all pixels, that have a non-background neighbor pixel, are equal. These equal pixels (connected components) get then the same label. There are multiple ways to define neighbors. The standard way is to use a "1-connectivity" (connect to neighbors on top/bottom/left/right, without diagonals).

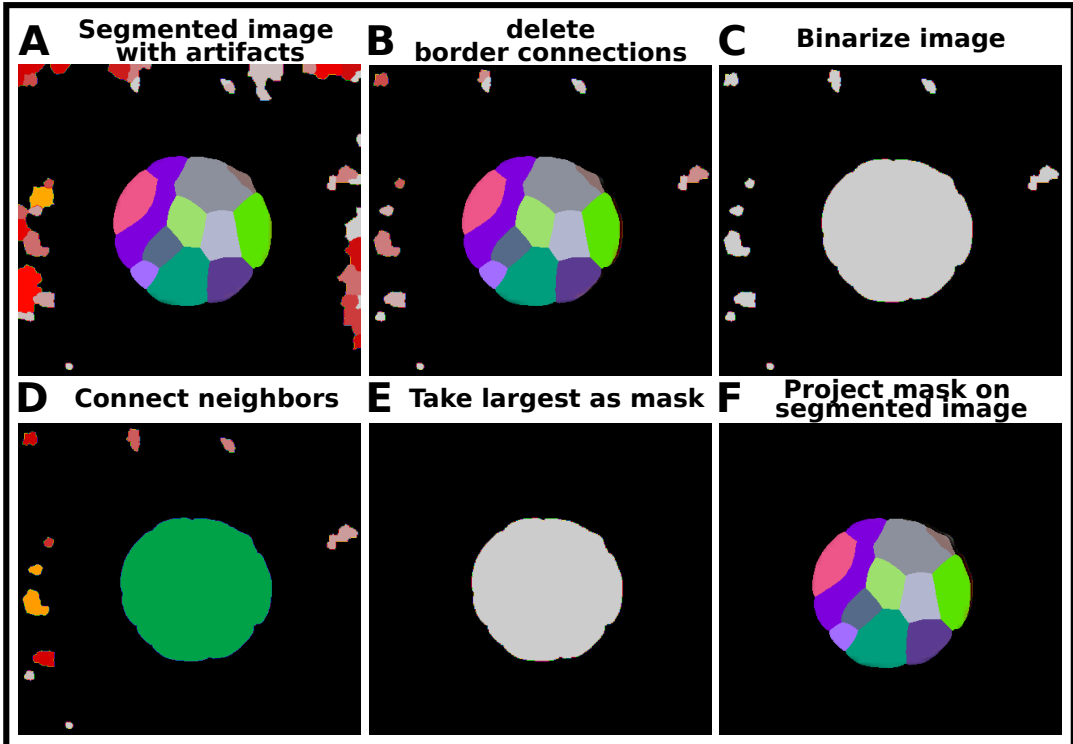


Figure 3.2: Artifact removal after PlantSeg instance segmentation. a) PlantSeg predictions with artifacts along the border. b) All contact points with the border are deleted. c) Binary image of 3D segmentation. d) CCL of objects in 3D. e) Largest label turns to a binary mask. f) Apply mask on input image.

Back to the artifact removal, the post-processing algorithm consist of 6 steps. In step one, the original image (3D) is opened (Figure 3.2 A) and all contacts with the border of the image are deleted (Figure 3.2 B). This step is connected to property 4.

In the second step, all non-zero elements are set to 1 (binary image, Figure 3.2 C). Now due to the property 3, CCL defines the organoid as one component and all artifacts as other components (Figure 3.2 D).

Based on the properties one and two, a volume measurement of the connected labels defines the largest object as an organoid. This one can be picked as a new mask (Figure 3.2 E) and the mask can be applied to the original image to get the artifact removed 3D image (Figure 3.2 F).

It can happen that there are more artifacts than cells in the captures. Then the la-

bel with the largest volume is the artifact and then the algorithm would exclude the organoid. This leads then to segmentation with thousands of cells. In this case, the result has to be discarded based on a threshold and the next highest volume has to be chosen. The threshold is defined by the user and is a (user guessed) a maximum number of cells.

This algorithm is sufficient to discard all wrong classifications outside the organoid. To discard wrong classifications inside the organoid, it needs another tool.

3.3.3 Combine single classification errors with the most likely neighbor

After removing artifacts which do not touch the organoid, it is now important to deal with artifacts inside the organoid. These objects are not artifacts, but rather wrong classifications or short "errors". They occur mostly above the organoid or below the organoid because SPIM has different intensity profiles here. These intensity profiles are unknown for PlantSeg. These "errors" (above, below, or inside the organoid) have the property that they are tiny (single z-slices). The "errors" can be seen in Figure 3.3 A (magenta) and the corresponding the number of pixels can be seen in Figure 3.3 B (magenta). The rest of the organoid is visualized and plotted in gray.

The classification between real cells and "error" is made arbitrary by introducing a threshold. The threshold here is chosen to be 1/3 of the weighted mean value of the sum over all pixels per label. It could be also chosen to be a minimum "volume", which the experimenter wants to define as a cell.

Once the "errors" are defined, they are merged with the most reasonable cell. There are two situations. Situation one is "errors" at the bottom or top of the organoid (Figure 3.3 A, C). Situation two are "errors" inside the organoid (Figure 3.3 A, D).

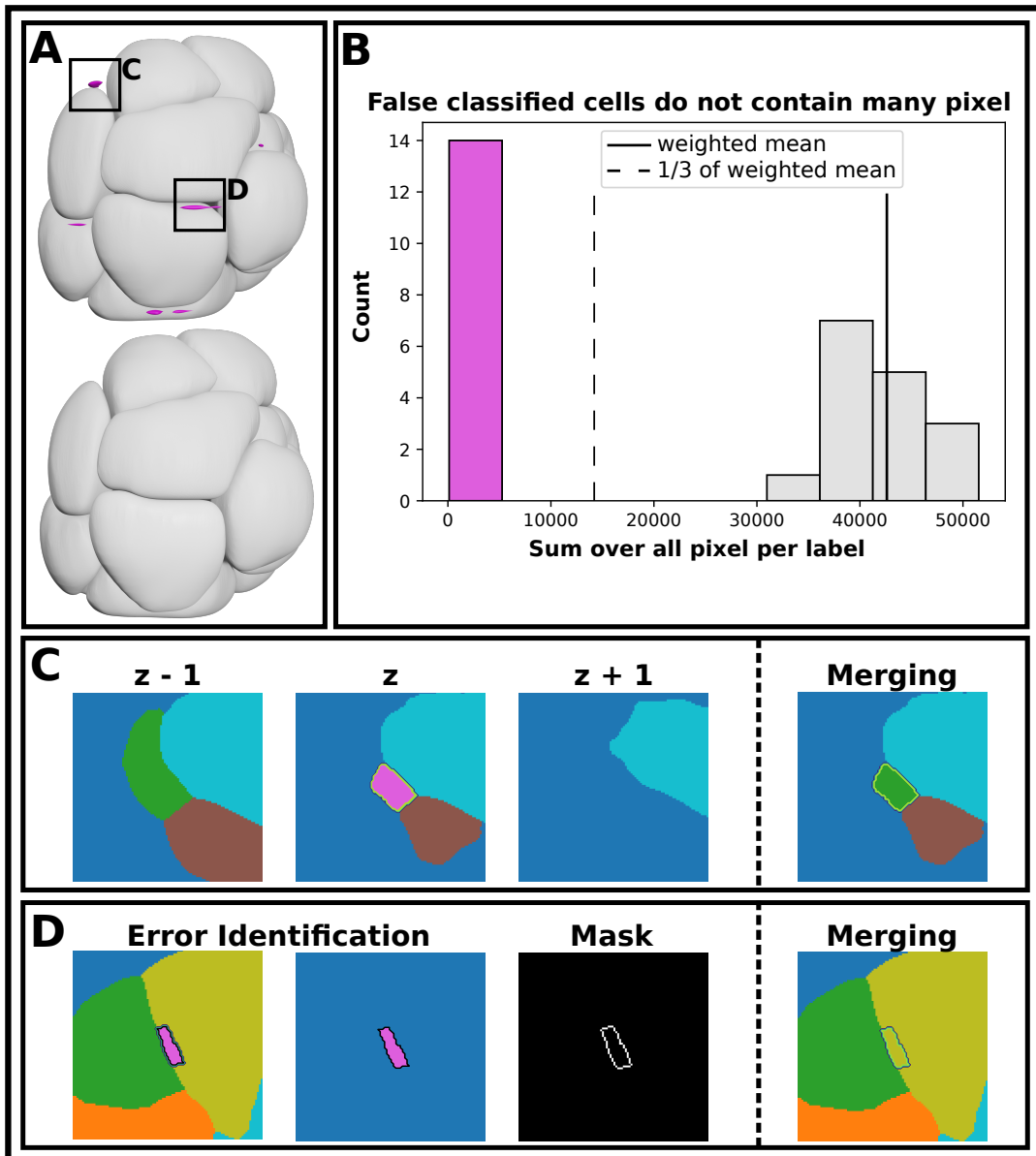


Figure 3.3: Merging of false classifications with real cells to obtain reasonable segmentation. A) Cells of the organoid before (top) and after (bottom) merging the false classified cells (magenta). The insets C and D are examples of a top event or events in between cells respectively. B) The distribution of the sum of all pixels that one label contains. The solid line is the weighted mean value of all measurements. The dotted line is the threshold between false classification (magenta) and correct classification (gray). The threshold is set to 1/3 of the weighted mean value of all measurements. C) Top (or bottom) events are detected by searching for the neighbor below ($z-1$) and the neighbor above ($z+1$) for a detected "error" (magenta, z). If the centroid (x, y, z) of the magenta object is in contact with the background in ($z+1$) or ($z-1$) then it will change its label to the label of the position ($x, y, z-1$) or ($x, y, z+1$) respectively (Merging magenta label to green label). D) "errors" inside the organoid are identified and isolated (magenta). The isolated object is expanded by one pixel and builds a mask. The mask is then used to count the neighbor labels. The label of the neighbor with the most contact to the "error" cell (most counts along the mask) will be applied to the error cell. The magenta "error" label is merged with the yellow neighbor cell.

Note: The boxes C and D are other examples than the inset C and D in box A.

Situation one (top-bottom) is solved by searching for "background" label below ($z-1$) or above ($z+1$) the cell (z) and "real" label above or below. In Figure 3.3 C, the "error" (magenta) in z has a "background" label above ($z+1$, dark blue) and a real cell label below ($z-1$, green) and is hence merged with the real cell. The "error" label then takes the label of the real cell and changes its color from magenta to green.

Situation two (in between) is solved by searching for and merging with the neighbor cell, which has the most contact points (Figure 3.3 D). First, the "error" has to be identified and extracted (magenta object). Then the object will be expanded by one pixel and transformed into a one-pixel-sized mask. The mask is then used to scan the neighbors. The neighbor cell with the most counts is the one with the most contact points. The label of this neighbor is then used to merge the "error" with this cell. In the example, the magenta cell detects more yellow neighbors than green neighbors and merges with the yellow neighbor consequently.

After applying these algorithms to the segmentation result, the final segmentation is close to reality (compare Figure 3.3 A, bottom). To measure the segmentation accuracy, one can use different measures.

3.3.4 Cell overlap calculation used as a measure for the segmentation accuracy and used for lineage tracing

After the post-processing of the instance segmentation results, the segmentation accuracy is measured with the VJI. The VJI is then also used to perform lineage tracing by simply changing the input. An implementation of the VJI and can be found in GitLab¹⁰ (Kar, 2022).

Volume averaged Jaccard Index

The VJI is a three-dimensional version of the Jaccard index, which is a measure for pixel overlap. The basic idea of the Jaccard index is, to count the accurately labeled pixels (which are not background) and to norm this (true positive) result by the amount of true positive and false positive pixels. True and false labeled pixels can be identified by using a manually annotated GT. Mathematically expressed with the overlap of GT with the predictions ($G \cap P$) and the complete area of GT and predictions ($G \cup P$):

$$JI = \left| \frac{G \cap P}{G \cup P} \right| \quad (1)$$

To measure the overlap in 3D one could directly sum up the equation 1 for all z-slices

¹⁰VJI GitLab: https://mosaic.gitlabpages.inria.fr/publications/seg_compare/evaluation.html

and norm them with the number of z-slices. Nevertheless, more accurate is the weighted summation of the Jaccard indices based on the cell volume (measured by using the GT). The mathematical formulation with the volume $|G_i|$ is described here:

$$VJI = \frac{\sum_{i=1}^N |G_i| \left| \frac{G_i \cap P_i}{G_i \cup P_i} \right|}{\sum_{i=1}^N |G_i|} \quad (2)$$

Lineage Tracing

The VJI is a measure for the overlap between a GT and a prediction for the same image. Lineage tracing is the connection between objects from one time step (T) to the next time step (T+1) for all time steps.

One way of connecting objects between these time steps is, to compare the overlay of all pixels from an object in (T) with an object in (T+1). This is possible by using the VJI from equation 2 and comparing the objects from (T) with the objects from (T+1) instead of the GT and the predictions (P) respectively (compare Figure 3.4).

In this figure one can see that the cells from time step (T+1) overlap with cells from time step (T). The cell from (T), which has the highest overlap with the cell from (T+1) transfers its label to the cell from (T+1).

Performing this step for all cells and time steps leads to cell-lineage tracing. The cell-lineage tracing based on the cell-cell overlap is more robust than the tracing based on the Center of Mass (COM) of the cells as one can see in Figure 3.4 on the bottom right.

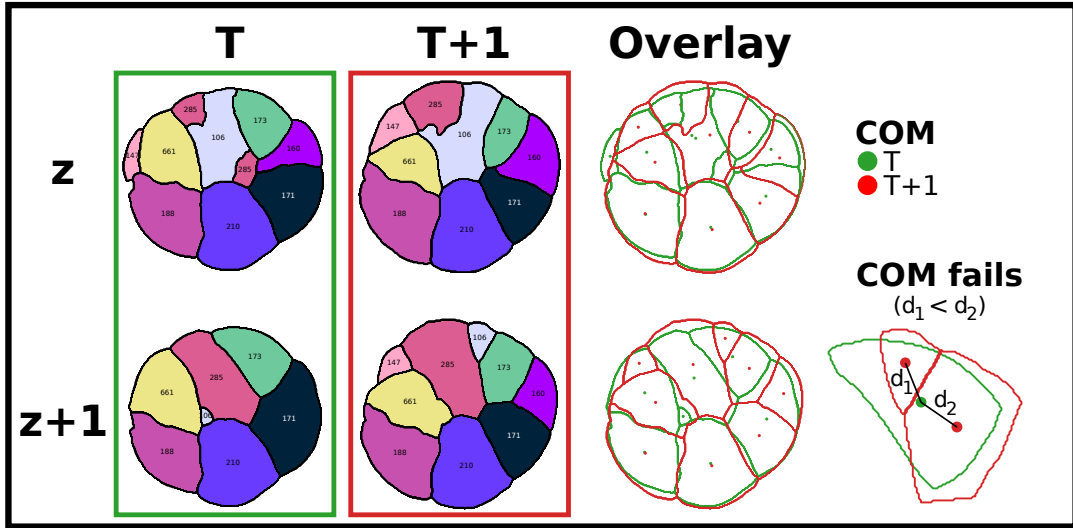


Figure 3.4: Lineage Tracing determined by the cell-cell overlap. Cell slices (z , $z+1$) are shown for the time steps (T, T+1) with already connected labels. The overlay shows the COM as well as the cell outlines from the time step (T) in green and (T+1) in red. The cell in (T+1) with the most overlap with the cell in (T) takes over the label of the corresponding cell. At the bottom right is a zoomed-in version of the overlay (T+1, $z+1$) where the COM gives a different result than the overlap.

3.3.5 Time information based post-processing to detect and remove segmentation errors

After removing artifacts from the instance segmentation, followed by merging minor misclassifications with the best fitting neighbor, there are still misclassifications left. These misclassifications can be seen by taking a look at the cell count over time (Figure 3.5 A). There one can see that peaks occur which suggests that single cells are added or removed for a single time steps. This is obviously a segmentation error in these cases. By taking a look at the example (inset), one can see that cells merge together at this point (2D example of a 3D problem). My attempt to fix these errors is based on the time information from the previous time step (T) followed by re-segmenting the time step ($T+1$) based on watershed.

Watershed

WS was first introduced by Serge Beuchert (Beuchert, 1979), and refined by several scientists. The final implementation of WS in scikit-image is based on the paper of Peer Neubert and Peter Protzel (Neubert, 2014).

The basic idea behind WS is strongly connected to the name itself. A watershed in real-life is the line that marks the boundary between two catchment areas of watercourses. Concretely it is the line that separates two areas from each other. For example, imagine a 2D image with pixel intensities as a topographical map, consisting of valleys (low pixel values) and hills (high pixel values). This map can then be flooded by water which will fill up all areas. Some areas are separated by a hill, in the beginning, so they are classified as different areas. Once the water level is raised high enough to flood the hills, the areas are connected with water. Back in the image analysis picture, this last step before flooding the areas is used to define the boundary line and to separate objects from each other.

Important for images with noise is to set constraints to the segmentation. A typically used case of WS is "Seeded Watershed", which means that one can set seeds into the image, which then start to fill the area until they touch each other. In such a way, one can make sure that only objects of interest are segmented.

Furthermore, WS can also be applied to already segmented data (or binary images). In these cases, it is common to define topography with the help of a distance matrix. The distance matrix of a 2D image is a 2D map, where every value is defined as the distance from the pixel to the closest border. Pixels outside the segmented part are zero. This leads to hills in the center of the segmentation and valleys at the border. Logically the inverse is used for performing WS.

Detection and re-segmentation of large merged cells

To detect and re-segment wrong segmentations it needs 5 steps, which are then repeated until no issues are left. The steps are shown in Figure 3.5.

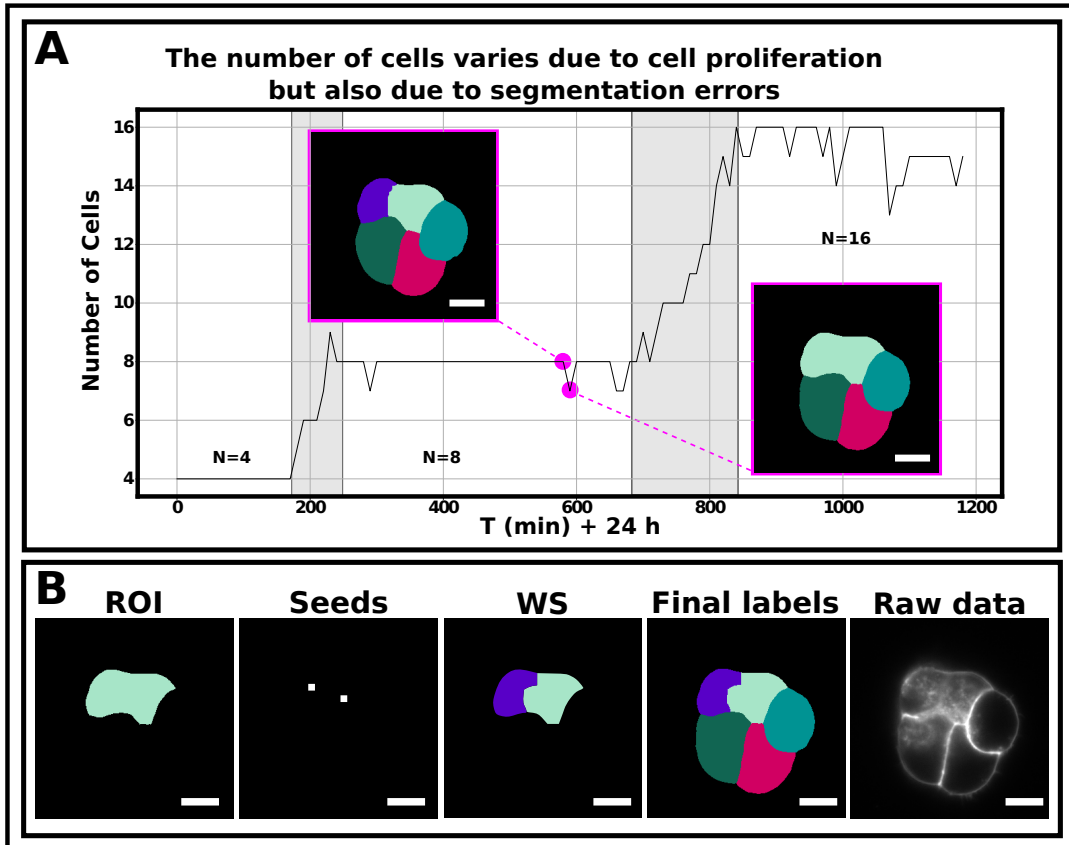


Figure 3.5: Watershed and time series based re-segmenting of wrong segmented, large, merged cells. A) Cell count within the embryonic development from $T = (0 + 24\text{h})$ up to $T = (20\text{h} + 24\text{h})$. The insets are examples of merged cells. B) Pipeline for re-segmenting the data with the help of seeded WS in the Region Of Interest (ROI). The scale bar is $10 \mu\text{m}$

- 1) Identify merging cells based on the end of the existence of one cell (similar to cell count) and the volume (Figure 3.5 A and Figure 4.2 A in section 4.3). The volume increases so that $V_{T+1} \approx V_{1,T} + V_{2,T}$. Isolate this area like in Figure 3.5 B, Region Of Interest.
- 2) Get the COMs of the previous time step (T) of the identified two cells (Figure 3.5 B, Seeds).
- 3) Use the COMs as seeds for 3D watershed to re-segment the cells (Figure 3.5 B, WS).
- 4) Overwrite the cells in ($T+1$) with the new data from (3) to get a full 3D segmentation of time step ($T+1$) (Figure 3.5 B, Final labels).
- 5) Apply lineage tracing again on the new data set.

6) Repeat these steps until all errors are fixed.

This algorithm makes sure that all merged cells are detected. Most of the detected cells are then correctly re-segmented like in the example in Figure 3.5.

Unfortunately, seeded WS is strongly dependent on the seed itself. The seed has to be placed at least inside the mask of the cell, optimally close to the center of the cell. Due to comparably slow movement of the organoid cells, this is mostly the case. Some situations though will not be segmentable with seeded WS, because the COM of (T) is not inside the COM of (T+1). This happens e.g. for non-convex shapes, like a cell that is winded around another cell and builds kind of "unfilled half moon". This also happens for cells that are completely surrounded by another cell. The COM seed in these cases is not inside the mask.

The here described limitation is nevertheless not influencing the results tremendously, because the analysis is performed by keeping the limitations in mind.

3.4 Data preparation for the quantification of single-cell parameters

The base for quantitative analysis is set with the fully automated segmentation pipeline, with lineage tracing. Starting from this point, parameters for the development of single cells can be obtained. For this, it needs always segmentation. Depending on the situation it needs also the membrane channel, the receptor channel, or both together. In the following parts, the parameter extraction will be described, beginning with the segmentation results and the membrane channel.

3.4.1 3D Mesh reconstruction, Volume and Surface area measurement

The segmented 3D data is actually "only" a stack of 2D images, which is acquired in different z heights (it is called 2.5 dimensional or pseudo-3D). To measure volumes, one has to construct a 3D mesh from them. This is done by interpolation between the z-slices (Sullivan, 2019). Interpolation is done by connecting the contour pixels of the slices with the ones from the next slices with triangular shapes. I am using scikit-image's marching cube¹¹ algorithm for this, together with trimesh¹².

This interpolation can be smoothed. Smoothing does not make the measurements more correct, so the smoothing is not applied in this pipeline to measure volume or surface area. Nevertheless, smoothing is applied when it comes to visualizing the data (for aesthetical reasons, see Figure 3.3 A). Hence, volume and surface area are measured on

¹¹Marching Cube: https://scikit-image.org/docs/stable/auto_examples/edges/plot_marching_cubes.html, 21.08.2022

¹²Trimesh: <https://trimesh.org/trimesh.html>, 21.08.2022

expanded z-slices (expansion by the factor z/x with the voxel sizes (x, y, z)).

Every cell is measured for every time step independently and the output is a table in the following format:

Table 3.3: Basic output structure of all performed measurements. The cell and time information is stored in every measurement, together with the extracted parameters (here: Volume, Area). This allows in the end to plot and merges all tables like a charm.

Cell	Time	Volume (μm^3)	Area (μm^2)	other parameters
1	0
1	:	:	:	:
1	T
:	:	:	:	:

3.4.2 Cell interface detection, classification, and analysis with respect to receptor and membrane concentration

It is important to detect and classify cell interfaces to finally quantify the cell interface dynamics during mouse epiblast organoid formation. This step bases on the accurate segmentation from chapter 3.3 (see Figure 3.6 A) and ends up in the quantification of fluorophores (from the membrane or receptor channel) along the cell interfaces during the embryonic development (see Figure 3.6 F).

The first step in this algorithm is, to convert the segmented image into a junction-classified image (see Figure 3.6 A-C). This is done by using a (3x3) kernel and screening over the 3D stacks, slice by slice. This results in a junction-classified image with basal junctions (green, one-cellular), lateral or apical junctions (orange, 2-cellular-junction (2J)), 3-cellular-junction (3J) (gray), and higher order junctions (pink).

Due to the kernel size, it is highly improbable (but possible) to detect junctions higher than 3rd order in this step. By taking a look in (B) or (C), one can see that it makes sense to define a 4-cellular-junction (4J) in this case. The easiest way for this decision is shown in the inset. The experimenter has to decide on a distance threshold d , which has to be falling below to be classified as a 4J. Then one can count the amount of 3Js which are below this threshold d to find out if the junction itself is 3, 4, 5, or more cellular (e.g. three 3J close together are actually a 5-cellular junction). This idea is connected to one issue, which I was not fixing yet, so in the analysis here, one has to be aware that 4Js contains measurements from 5 or higher order junctions too.

Before making the final measurement, the junctions have to be diluted to make the measurement over a larger area and hereby more robust (see Figure 3.6 D). For this,

the 3D images are diluted with a 2D kernel, so that no dilution happens along z. The dilution starts from the lowest order junction and then continues with the next higher ordered junctions. This ensures that no junction gets lost and that lower order junctions do not measure the signals in places where higher order junctions are located.

In the end, the measurement is performed in either the receptor channel as one can see in the Figure or in the membrane channel. One example result is shown in Figure 3.6 F, to visualize the output of the measurements. The analysis of this results is made in chapter 4.6. One can see the distribution (violin plot) of all measured intensities along the junctions, sorted by the junction order from left to right (colors match the description). This analysis is then made for all time steps and for the membrane and receptor channel.

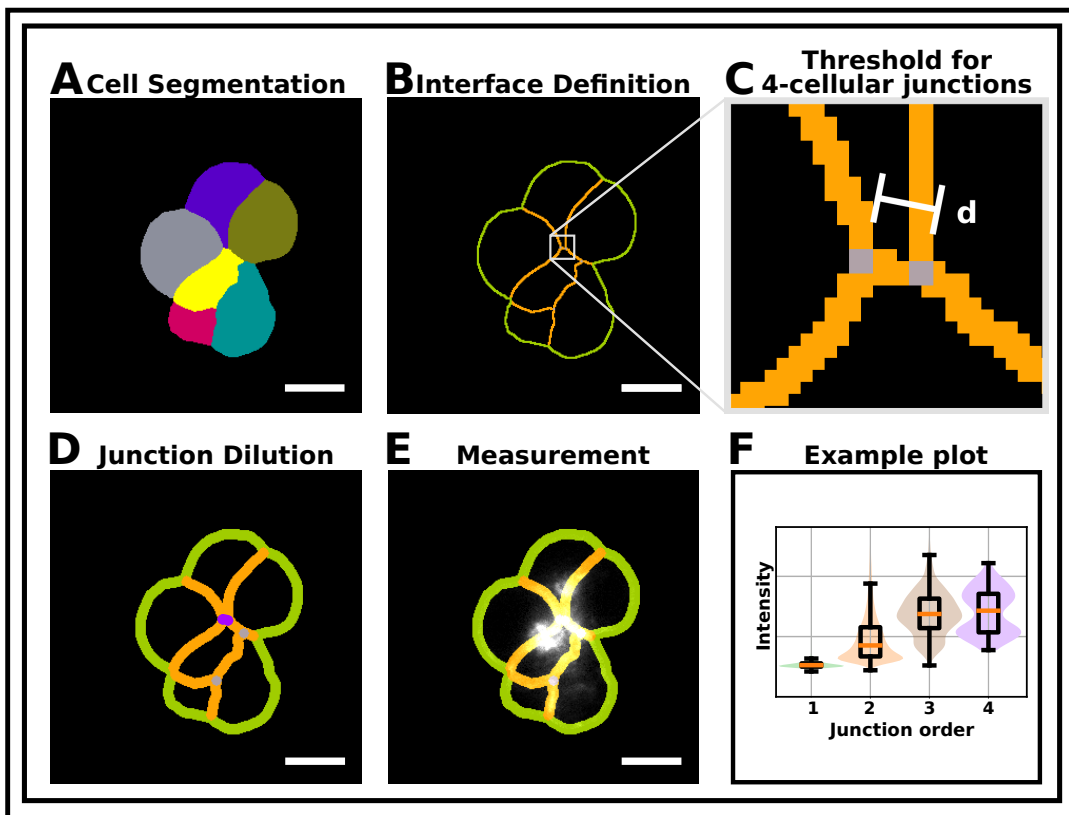


Figure 3.6: Algorithm for cell interface detection, classification and measuring for mono-, bi-, tri- and multi-cellular junctions. A) Fully segmented data. B) A junction map for mainly 1-cellular-junctions (1Js), 2Js, 3Js, but also higher order junctions. C) The amount of 4Js can be artificially increased by applying a distance (d) threshold to 3Js. Events which are below this threshold are increased from 3rd to 4th order. This can be done for higher orders too. D) Dilute all junctions (beginning from the lowest order) to cover a larger area and be more robust in measurements. E) Performance of the measurement in the receptor or membrane channel. The scale bar is $10 \mu\text{m}$. F) Example result of the measurement in the receptor channel by applying the junction map (in 3D). The measured pixel intensities are plotted against the junction order.

3.4.3 Background subtraction in the Podxl captures

To measure fluorophore concentrations, it is necessary to remove unwanted signals from the image. This is especially important in the receptor channel (Figure 3.7 A), because there exist very low concentrations along the basal side, which would be covered by background noise. To remove this noise, a threshold is applied. This threshold is based on the background signal, but not on the signal of the organoid itself. To do so, it needs 4 steps.

Step 1 is to apply a Difference of Gaussian operation ($\sigma_{\text{high}} = 20$, $\sigma_{\text{low}} = 0$) on the image. Step 2 is to use the inverse of the segmentation to define the background profile. Step 3 is to define the mean and standard deviation of this profile as the threshold. In the last step, these threshold images are projected on the original data again. The result is a common threshold (Figure 3.7 B). which is based on the individual background profiles of the images.

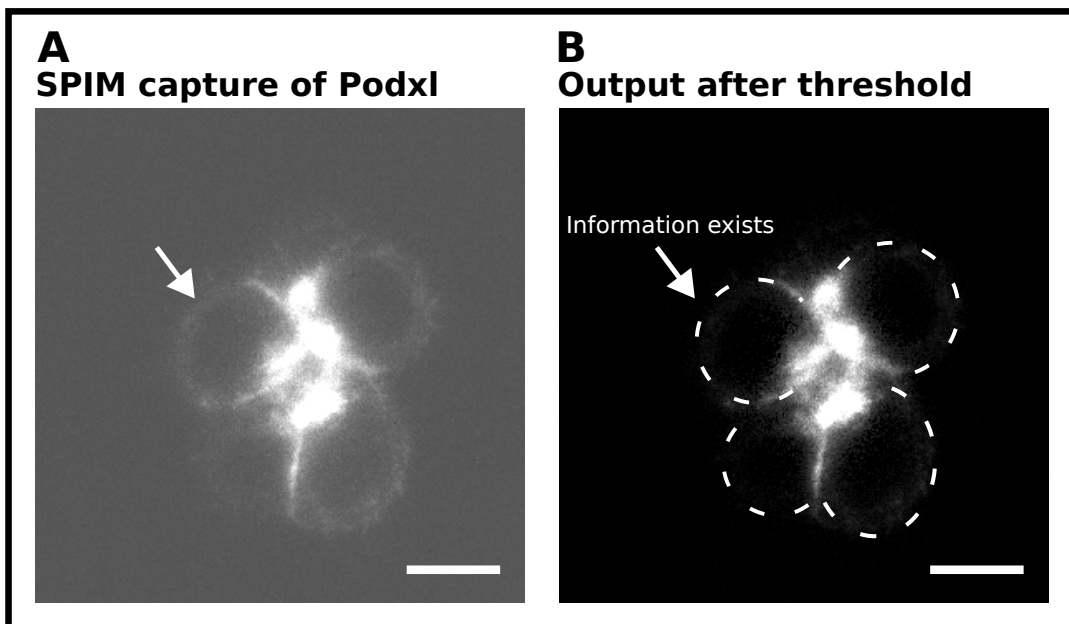


Figure 3.7: Segmentation-based background subtraction to filter out noise from the receptor captures. A) SPIM capture of Podxl with low Signal-to-Noise at the basal side. B) Background removed capture which still contains basal receptor intensities. The scale bar is 10 μm .

3.4.4 Center of Mass based tracking of Podocalyxin

For the analysis of the polarization of the cell, it becomes important to track the receptor flow. The receptor itself exists in nearly all pixels that are connected to the organoid. This is an enormous amount of data. To reduce the complexity of polarization measurements, the receptor intensity is represented cell-wise as one position. This

Quantification and statistical analysis

position is the COM of all Podxl (\tilde{r}_{COM}) within a cell (a cell has N voxels). To get the COM of the intensity (I), one has to calculate:

$$\vec{r}_{COM,Cell} = \frac{\sum_i^N I_i \cdot \vec{r}_i}{\sum_i^N I_i} \quad (3)$$

To estimate the COM of the complete organoid, one has to do this process for all cells at the same time.

In both cases, the case of single cell polarities and the case of an organoid COM of Podxl, one has to be careful about symmetries and averages. One cell can have multiple Podxl accumulation points, but the COM would only represent one point. This point could then also be in the middle of the several actual points.

3.5 Quantification and statistical analysis

Every measurement is connected to statistical and methodical uncertainty. All performed measurements in this experiment are based on the video captures and the segmentation accuracy. The video captures are limited by the voxel size as a digital constraint and by the resolution as a physical constraint. In practice, the limitation of our data is the voxel size.

The segmentation accuracy is at our level of precision harder to describe, because the post-processed results reach nearly expert accuracy. This leads to the fact that the GT is not tremendously better than the automated predictions and that the definition of accuracy needs to be judged on other criteria. Temporal errors can be neglected in the slow-moving system.

Hypothesis tests

To test the hypotheses if the two groups are different, I am performing parametric hypothesis tests for data with underlying Gaussian distribution and non-parametric hypothesis tests for data without underlying Gaussian distribution. Data with a small sample size and underlying Gaussian distribution are tested with the t-test. The assumptions here are (i) the distributions can be approximated by the mean (very important) (ii) equal standard deviations between samples (important because of powerful outliers) (iii) samples are representative and (iv) independent observations.

If the data can not fulfill these assumptions, I am using non-parametric tests. These are the Kruskal-Wallis and the Dunn-test. These are multi-sample, rank-based tests. Non-parametric tests are less powerful than parametric tests, but this can be handled by having a larger sample size. For multi-comparison corrections, I am using the Bonferroni correction. The assumptions for the Kruskal-Wallis test are (i) the data is based

on an ordinal or continuous variable (ii) observations are independent (iii) distributions have a similar shape.

If the Kruskal-Wallis test shows significant differences in all groups, then the Dunn test with Bonferroni correction is performed to test the groups independently.

Typical misconception about hypothesis tests

Hypothesis tests are performed between two or more groups, based on a common variable. One can never test if groups are different, but one can test if groups tend to be equal or not equal. Actually one can only test how probable it is to be wrong with the statement that groups are not equal when they are indeed equal. This probability is described by the p-value.

This p-value is mostly set to 0.05 or 0.001 and the statements are called "significant" or "not significant" if they are below or above this value respectively.

So instead of writing:

Groups are significant, not equal. (With the idea in mind, that they could be equal and the result came just by chance)

I will write in this thesis:

Groups are (significantly) different.

Linear regression

For the measurement of some parameters, I am using the method of linear regression. The R^2 value of this regression is a measure of the accuracy of this approximation. The R^2 value is defined as

$$R^2 = 1 - \frac{\sum(y_{true} - y_{pred})^2}{\sum(y_{true} - y_{mean})^2} \quad (4)$$

and is the fraction of explained variance in the data. E.g. $R^2 = 0.98$ means that 98 percent of the variation in the data can be explained by linear regression.

4 Results

Within this thesis, I developed a pipeline to quantify cell interface dynamics and more during the mouse epiblast organoid formation. It is based on image segmentation and post-processing for confocal microscopy data. Imaging, segmentation, and quantification results are presented in this order and give biological insights on a single cell level, like never before.

4.1 3D Mouse epiblast organoids develop from single cells to organoids with lumen

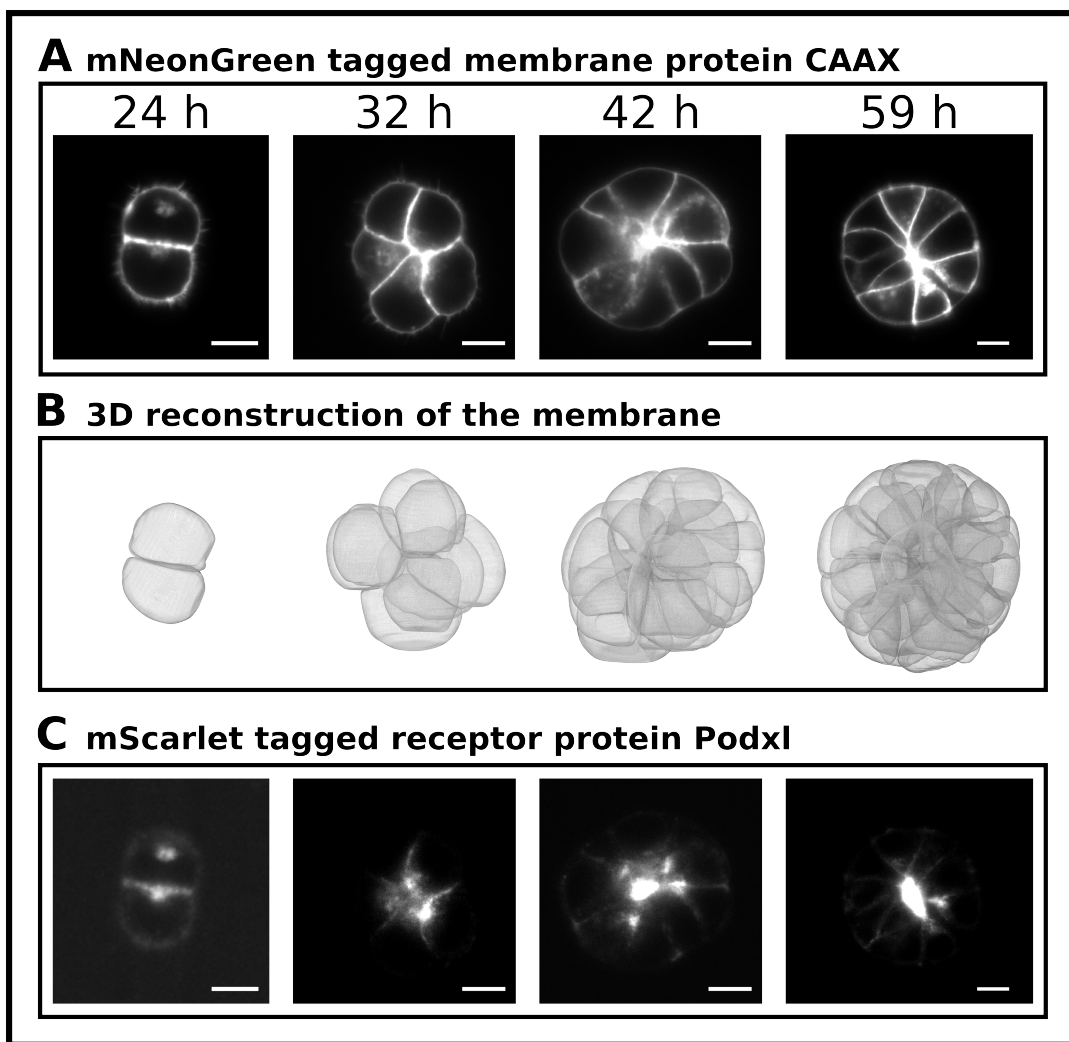


Figure 4.1: The stages of mouse Embryonic Stem Cell development for CAAAX and Podxl captures from single cells to organoid rosettes. A) SPIM image of NG, attached to CAAAX. B) 3D reconstruction of the membrane. C) SPIM image of mScarlet, attached to Podxl.

The images are snapshots of different organoids. The images in A and C show a single z-slice. The length of the scale bar is 10 μm

First of all, the 3D mouse epiblast organoids were prepared as described in section 3.1 and imaged like in section 3.2. This results in data sets, which cover the stages of single cells (24 hours after seeding the first cell) up to early lumen formation states (42 hours after seeding the first cell) and beyond. This can be seen in Figure 4.1. In this Figure is the membrane channel (A), the 3D reconstruction (B), and the receptor channel (C) visible. One can see the growth of the organoid in general due to proliferation. In A, CAAX can be seen. Due to its homogeneous distribution, the visible intensity along the basal side (1-cellular-junction (1J)) is half as intense as the intensity along the 2J. A more detailed analysis is in section 4.5.

In A, one can see also the production and transport of new produced CAAX inside the cell.

The organoid rosette formation is reached in time step 42 with the COM close to the geometrical center of the organoid. By taking a look in C, one can see that the membrane-attached receptor protein Podxl accumulates in these regions too. The center of the rosette becomes the point of lumen formation.

By comparing the 24 h Podxl capture with the others, one can see that the receptor is transported away from the basal side and accumulates close to the geometrical center. This happens due to intracellular transport or membrane diffusion.

The quantitative analysis of the data is then performed by using instance segmentation. The data which is mainly analyzed is a data set by Yara, which covers the time from 24 h up to 44 h. The principle can be applied to all data sets.

4.2 Automated segmentation post-processing for improving accuracy and quantifying 4D segmented data is easier than ever before

To analyze the 3D SPIM data shown in Figure 4.1 A, B. I developed a pipeline that takes segmentation images as input and post-processes them in a way that they are biologically more meaningful. This is described in detail in section 3.3. The algorithms are written for 3D data, but they can be adapted to 2D data as well. Additionally, it is post-processing, so the algorithms are applicable even to not SPIM and not organoid data if the user decides that it makes sense.

The quantification of the data in both microscopy channels is automated too. This is described in section 3.4. So in general, the analysis of a segmented 3D image over several time steps is now automated and needs a couple of seconds for one time step and around 30 min for a time series of 120 images (by taking the time of a user into account). The run time itself is approximately 5-10 minutes.

After running the pipeline, one gets an excellent segmentation together with measure-

mESCs proliferate and self-organize from a single cell to a 3D epiblast organoid with a single lumen

ments in the membrane channel, the receptor channel, and in both together. These measurements are sorted and easily accessible with python, excel, or any other software that can read csv files.

Once the program is included in a single script, it is user-friendly, because it needs nearly no parameters to tune. The program is able to run on multiple cores and on GPUs, which makes it even faster when choosing the right software. To sum up, this program helps scientists to analyze and quantify 4D data fast, reliable, and objective.

4.3 mESCs proliferate and self-organize from a single cell to a 3D epiblast organoid with a single lumen

Using the segmentation algorithm described in section 3.3 allows for analyzing the morphology of the single cells within an organoid. By taking a look at the change in the cell volume over time (Figure 4.2) it is possible to define the volume growth rate of the cells at different times of development. In Figure 4.2 A, one can see that the volume of all cells increases linearly until the cells divide. Quantification of the growth rate at 3 time intervals $T \in [0, 180], [220, 700], [900, 1200]$ reveals that the volume growth rates are not significantly different from each other (t-test, compare Figure 4.2 B and Table 4.1). Hence cell volumes increase at the same rate for each subsequent cell cycle throughout organoid development.

The t-test was made under the assumptions that (i) the distributions can be approximated by the mean, (ii) the standard deviations are similar, (iii) the samples are representative, and (iv) observations are independent. By taking a look at Table 4.1 one can see that the requirements are barely fulfilled and one has to analyze more cells from several organoids to allow stronger statements.

Besides this, the cells grow with an average volume growth rate of $(2.60 \pm 0.86) \mu\text{m}^3/\text{min}$. This might be due to space constraints, which are related to external pressures from the outside matrix and from the other cells. In future experiments, one could measure the volume or area growth rate depending on the nutrient or the growth rate depending on external pressure induced by matrigel stiffness.

The surface grows with $(0.88 \pm 0.71) \mu\text{m}^2/\text{min}$, measured in the same way (there are also no significant differences between the growth rates of different intervals).

In total, this means, that a cell needs to produce an amount of membrane that is equivalent to an area of $0.88 \mu\text{m}^2$ in every minute under the assumption that the membrane is not folded. The folded membrane is not segmented as such.

Within this thesis is no automated way to split up wrongly merged cells (cells which are visible as outliers in Figure 4.2 A). Hence it is not possible to analyze the start and end volume of a cell automatically. Analyzing these volumes would be necessary to test

the hypothesis (i) if daughter cells at later development states are larger than daughter cells at early development states (compare V_{\min}) or (the hypothesis (ii) if daughter cells grow larger than the mother cells (compare V_{\max}) or if cell divisions happen at a certain maximum volume, which inherited by the mother cell.

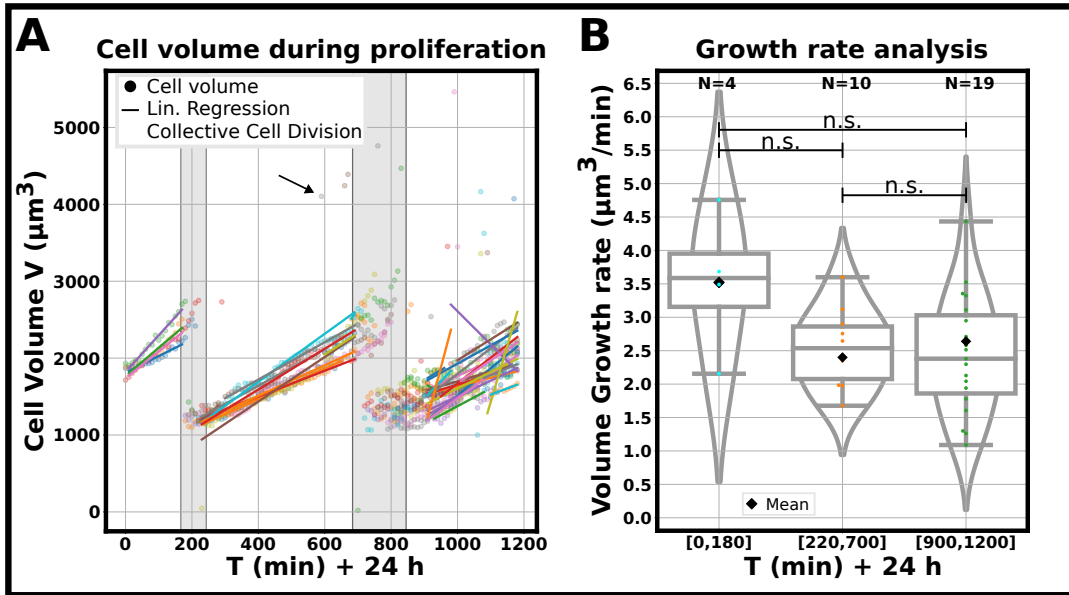


Figure 4.2: Cells within one organoid grow continuously with the same growth rate. A) Volume measurement (dots) of single cells during embryonic development from 24 hours ($T=0$) up to 44 hours ($T=1200$). The solid lines are linear regressions in the intervals $T \in [0, 180]$, $[220, 700]$, $[900, 1200]$ min. The arrow points to merged cells ($V=V_1 + V_2$). The gray tube is the time frame in which cell divisions happen collectively. B) Volume growth rate, calculated from the linear regression in A after removing outliers (above/below the upper/lower whiskers). The black squares represent the mean growth rate, and the solid line in the box plot represents the median growth rate. N is the number of measured growth rates after removing outliers. The p-value is obtained via t-test. n.s.: $p > 0.05$

Table 4.1: Descriptive statistics for the volume growth rate evaluation of Figure 4.2. The largest interval represents all data points after proving that the growth rates are not significantly different.

Interval (min + 24h)	[0,180]	[220,700]	[900,1200]	[0,1200]
N	4	10	19	33
μ ($\mu\text{m}^3/\text{min}$)	3.52	2.40	2.64	2.60
Median ($\mu\text{m}^3/\text{min}$)	3.59	2.16	2.55	2.51
σ ($\mu\text{m}^3/\text{min}$)	0.92	0.73	0.57	0.86

The pluripotent exit and the start of differentiation leads to a tremendous expression of Podocalyxin

4.4 The pluripotent exit and the start of differentiation leads to a tremendous expression of Podocalyxin

With the correct segmentation, it is now possible to make cell-based measurements of the receptor production during the cell cycles of the developing tissue. For doing so, I again split up the data manually into 3 regions (like in section 4.3) to analyze them independently. These regions can be seen in Figure 4.3. First of all, the overall receptor occurrence inside the organoid can be seen in Figure 4.3 A. Here one can see that $dI/dt > 0$ for all 3 regions (linear approximation with $R^2 \approx 1$), which describes a permanent Podxl production during all cell cycles. Production means that more receptor is produced (cell internally or along the membrane) than it is digested. For more information about receptor production, trafficking and digestion, look up Podxl membrane trafficking (This topic would pass the scope of this thesis).

In Figure 4.3 A one can also see that the production rate increases from cycle to cycle. Nevertheless, the underlying data does not show a significant difference between these 3 groups, consisting of 4, 8, and 16 cells (tested with a t-test). That means that the production rate is equal

Using the segmentation of the cells allows to track the single cell Podxl expression. These expressions are shown in Figure 4.3 B in gray color. Here one can see that cells in the first cycle ($T = 0$ min up to $T = 180$ min) can either produce, reduce or keep their receptor concentration over time. On average (black line and cyan linear approximation) they produce Podxl. After the cell division, the single cells seem to express Podxl with a higher rate and there is not a single cell that keeps the concentration constant or even decreases it. Again, all differences in this plot are not significant, due to the number of data points. Nevertheless, the tendency is visible.

In the last interval (yellow), the single cell behavior can not be tracked anymore, because even the best segmentation can not split up a lumen formation side (Figure 4.1 A and C, 42 h or 59 h, bright white dot in the center) correctly to the neighbor cells. Hence, one cell gets more of the lumen assigned and another cell less. In this interval, the average single-cell Podxl expression is considered without single cell information.

To test, if the receptor concentration increases because of the increased cell volume, the intensity is normalized with the volume (Figure 4.3 C). A constant value here means that the concentration stays constant under cell volume growth. In the first interval, this seems to be the case on average, so that the concentration of Podxl is conserved before the division. After the cell division, the receptor concentration increases drastically and it seems to even end up in a saturation limit (which could be around 3 times the beginning concentration).

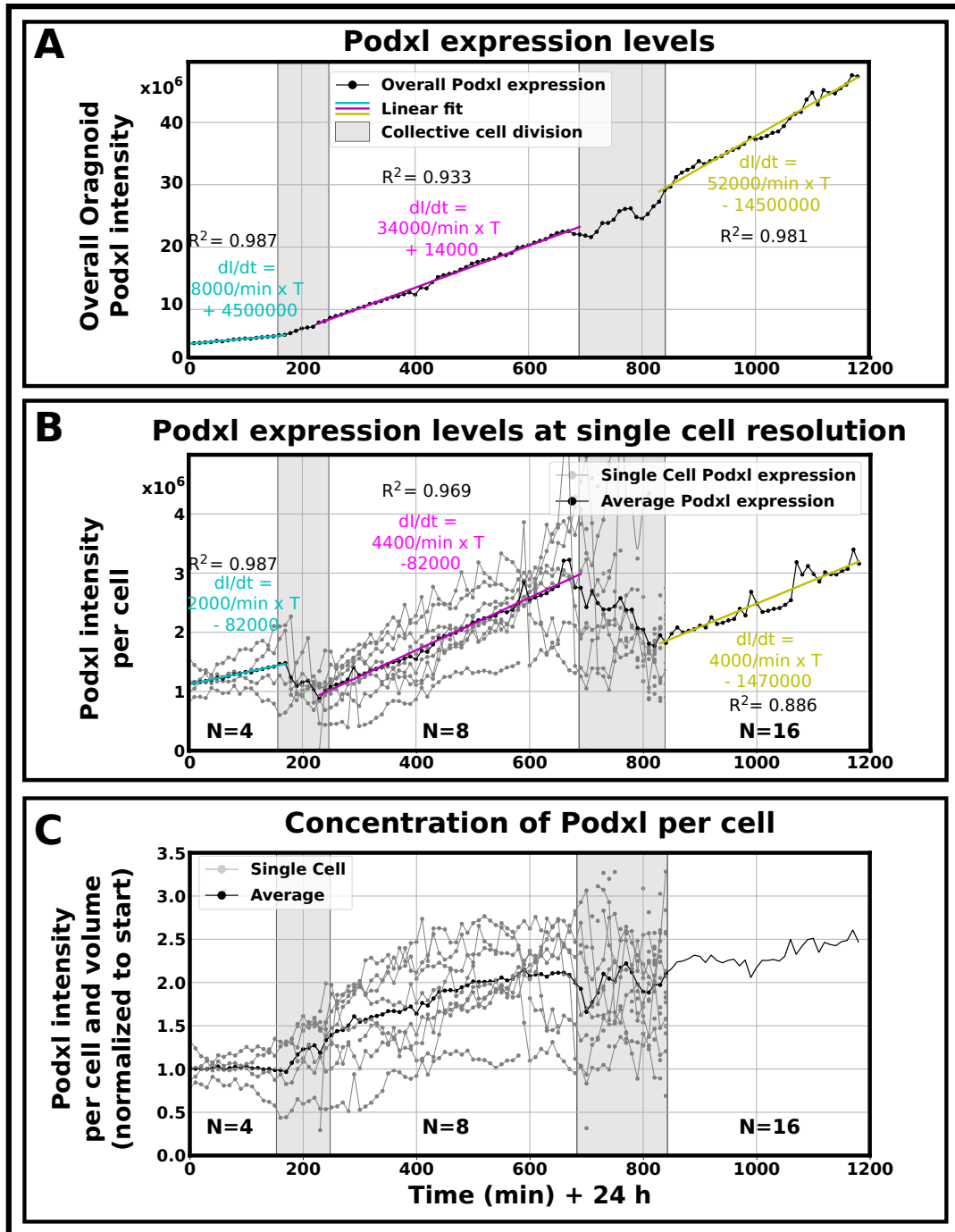


Figure 4.3: The pluripotent exit of the cell is the starting point of tremendous receptor production. A) Organoid overall Podxl intensity (molecules per voxel) over time, with linear approximations in the 3 intervals (cyan, magenta, yellow) between cell divisions (gray areas). B) Single-cell Podxl expression (gray line with dots) and the average of the cells (black line with dots). C) Podxl concentration (intensity per volume of the single cells), normalized with respect to the first average value.

In all plots, the complete receptor intensity within the cells (or organoid) is measured, which consists of internalized and membrane Podxl. Single-cell observations in the last interval suffer from segmentation accuracy and are hidden. N is the number of cells in the interval.

Homogeneously distributed proteins are n-fold more concentrated in n-cellular junctions than in 1-cellular junctions

To sum up, it looks like the cells of the organoid change the Podxl expression rate after the first interval. This change in Podxl expression rate could be initialized by the exit from the pluripotent state (Bodak, 2017; Cirera-Salinas, 2017). Cell division could be the trigger for this process. After the cell division, the single cells and hence the organoid, produce a tremendous amount of Podxl which increases the concentration in the cells. After 1200 min + 24 h, the concentration saturation seems to be not reached yet. At this time, the lumen is already visible.

Nevertheless, the amount of data is not sufficient to see a significant difference between the intervals ($p>0.05$, t-test).

In the differentiation step, Podxl will be used as membrane protein to initiate lumen formation, so it will be transported to the membrane. The enrichment of Podxl along the cell interfaces has to be studied separately and is the main part of the next topics.

4.5 Homogeneously distributed proteins are n-fold more concentrated in n-cellular junctions than in 1-cellular junctions

Using the junction detection from section 3.4.2 allows to track the distribution of membrane protein. The membrane protein CAAX is known to be homogeneously distributed along the membrane surface. This means that the concentration of the protein along cell-interfaces would be (in ideal case) always a multiple of the concentration along a single junction. For a n-cellular junction, one would expect the n-fold concentration than in a 1-cellular junction (basal side). To show this, the membrane intensity along the junctions was measured for every time step (see Figure 4.4).

For a single time step (Figure 4.4 A), one can see that the intensity (\propto concentration) of the membrane increases by 2.29 for a transition from a 1- to a 2- cellular junction. It increases by 3.81 or 3.97 for the transition from 1-cellular to 3- and 4- cellular junctions respectively. Whereas the groups marked with **** are significantly different, the group 3 and 4 can be considered as equal. Hence the 2.29 fold concentration increase can be connected to the change from a 1-, to a 2- cellular junction. The 3.81 up to 3.97 fold concentration increase can be connected to the change from a 1- cellular junction to junctions higher than 2-cellular.

Figure 4.4 B shows the median membrane intensity for all junctions and all time steps, with the expected behavior plotted in the black dashed line. The black crosses mark all data points, in which 3- and 4- cellular junctions can not be distinguished. Here the truth would be a combination from both values. Nevertheless, the data of 3J and 4J is plotted as independent in this points.

Beginning by the lowest order junction, one can see that the membrane intensity decreases continuously with time, having small deviations at the cell division events

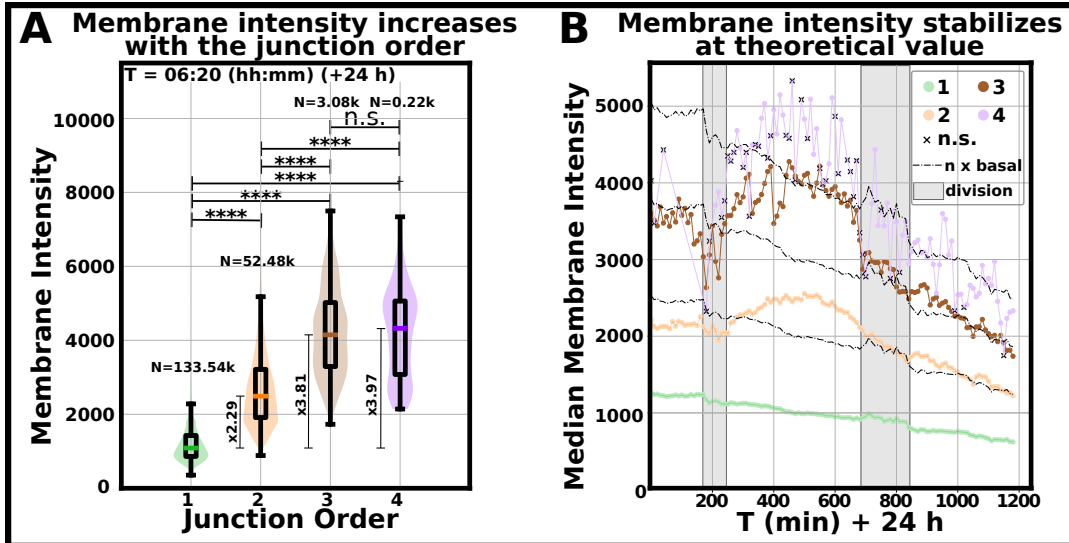


Figure 4.4: The protein concentration increases step wise with the junction order. A) The membrane intensity is plotted with respect to the junction order. The amount of analyzed voxels is N. The differences between the plots are significant (***, $p<0.001$, Dunn test) or not significant (n.s., $p>0.05$, Dunn test). The quotient between the junction median values with respect to the basal junction is plotted next to the violin plots.

B) Plot of the median value of the distribution from A for all time steps. The 4 junction groups are plotted in the same colors like in A. The black crosses mark the points in which the groups 3J and 4J are equal (n.s.). The dashed line shows the expectation based on the idea of a homogeneous protein in a flat membrane, where the concentration is proportional to the number (n) of membrane layers (n times basal intensity).

(around 200 min and 800 min). The intensity decreases, because of (a) photo bleaching, (b) the growing number of the cells and hence a reduced entry of light to all layers, which is connected to less activation light for the fluorophores, and (c) it could be connected to a lower expression of genes in the daughter cells (with respect to the high expression of the mother stem cell).

The membrane intensity along 2-cellular junctions is in the beginning (<300 in) lower, in the middle (>300 min, <700 min) higher and in the end (>700 min) equal to the expectation. This behavior can be seen for all types of junctions with junction order > 1 .

The higher concentration in the middle interval starts after the cell division and could come due to membrane folding. This folding reaches its maximum at the peak around $T = 500$ min, which is followed by a splitting up of membrane concentrations which would be expected.

Interestingly, this process can also be seen in the 3-and 4-cellular junctions (which can not be distinguished at the crossed time steps). In their cases the phenomena even

Non-homogeneously distributed apical receptor protein is higher concentrated in higher order junctions than in lower order junctions

reveals that the concentration of the 3- and 4-cellular junctions is as high as one would expect from 4-cellular junctions.

Fascinatingly, in the last interval, after the second here measured cell division, the junctions behave nearly exactly as expected. This means that n-cellular junctions have the n-fold concentration of protein as the 1-cellular junction. All junction types can be distinguished in most of the time steps in this interval.

To sum this up, it looks like membrane protein CAAX is in the beginning approximately homogeneously distributed. During the development, the concentrations of CAAX increases unexpectedly high, even as high as one would expect from the next higher junction. This could be explained by membrane folding. After this, the concentration in the junctions nearly perfectly split up into the concentrations which would be expected.

With knowledge about the distribution of homogeneous protein along the cell interfaces, it is now possible to analyze the distribution of Podxl along the cell interfaces.

4.6 Non-homogeneously distributed apical receptor protein is higher concentrated in higher order junctions than in lower order junctions

With the same method as before, the Podxl enrichment along the cell interfaces is measured (see Figure 4.5 A and B). In these Figures one can see that the intensity, depending on the junction order, increases again. This time even more tremendously. Partly, the receptor concentration in 2J is 6 times higher than in 1J. Also some trends look similar to the CAAX analysis. So for example the trend of enriching protein in the second interval in 2J and 3J/4J and splitting up the junctions in the last interval to distinguishable 3J and 4J.

This observations can now be used to test, if Podxl is homogeneously (like CAAX) or inhomogeneously distributed. From previous studies it is already known that Podxl is transported towards the apical side (Bryant, 2014), which means that this receptor would reach highest concentration at the apical side. This has to be quantified for mESC organoids. With the results from section 4.5 it is clear that the protein concentration increases with the junction order. Hence the data has to be corrected by this effect. The hypothesis is that the concentration of the protein Podxl increases more than a homogeneously distributed protein like CAAX would do. The null hypothesis is hence: H_0 : The change in concentration (\propto intensity) of Podxl by increasing the junction number, is equal to the change in concentration of the homogeneously distributed protein CAAX.

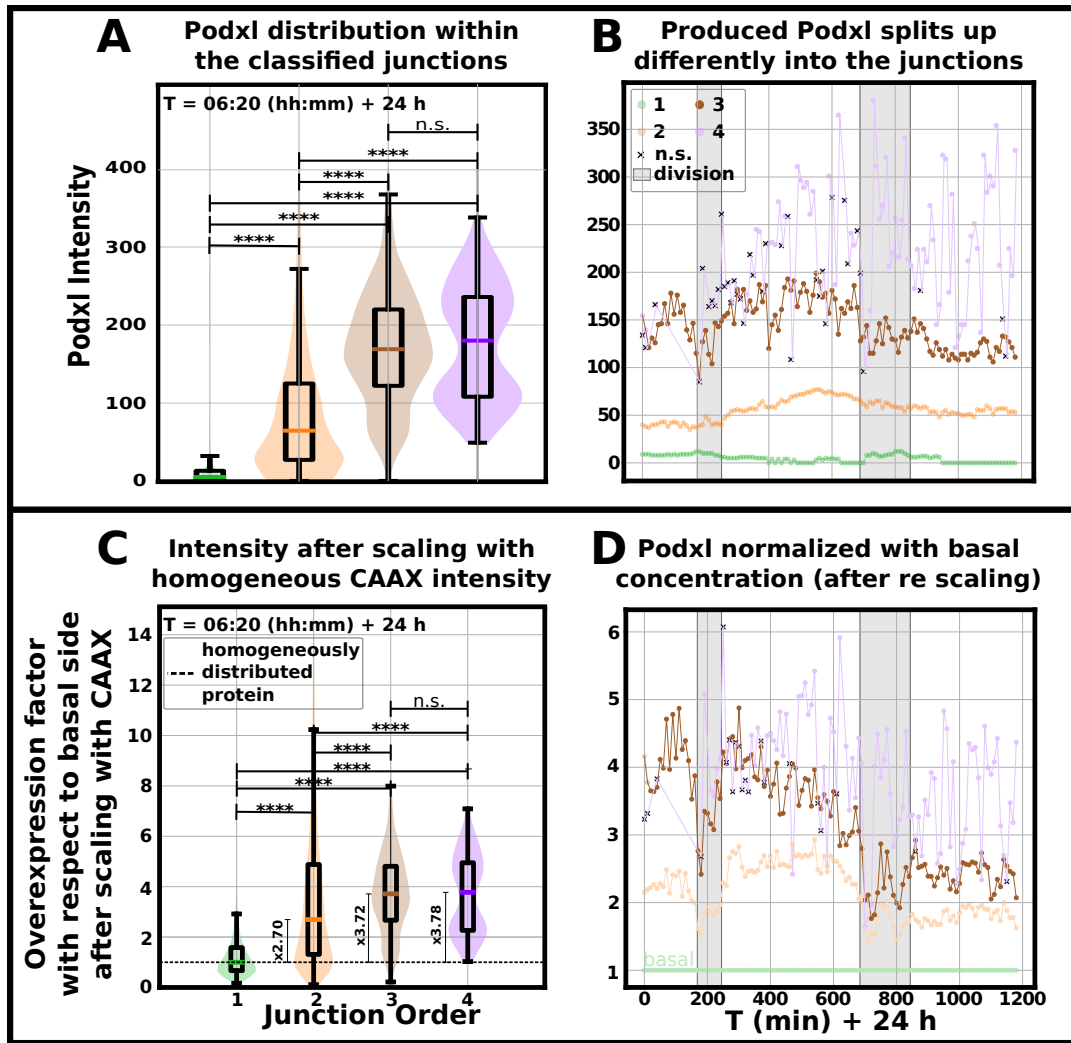


Figure 4.5: Non-homogeneously distributed receptor protein enriches in higher order junctions. A) Podxl intensity measurement depending on the junction order. The line in the box plot defines the median value, which is used in B. B) Median Podxl intensity for the mESC development. Gray areas are times in which cell divisions happen. Black crosses define not significant differences between 3J and 4J. C) Re-scaled and normalized intensities from A. Re-scaled with factors from Figure 4.4 A. Normalization with the basal side. The black dotted line represents the expectation for a homogeneously distributed protein like CAAX after re-scaling and normalization. D) Time development of C with the same principal as in B. The Kruskal-Wallis test showed significant differences between the data itself. The Dunn test gave either $p > 0.05$, n.s. or $p < 0.001$, ****. The number of measurements is the same as in Figure 4.4.

The measurement of the receptor intensity along the cell interfaces is shown in Figure 4.5. A and B show the absolute measured intensity and C and D show the re-scaled and normalized intensity. The intensity is re-scaled with the factors from the membrane analysis and the normalization happens with respect to the basal side.

By taking a look at A and B, one can already see that the intensity between junctions increases more than for the homogeneous protein (e.g. the median concentration of

Cells enrich Podocalyxin close to the geometrical center of the organoid, but still vary its exact position

the 1-cellular junction is 6 times less than the median concentration of the 2-cellular junction). After re-scaling with the factor from the membrane channel (factor between 1J and 2J is 2.29) an effective overexpression factor of 2.70 is reached (see Figures 4.4 A and 4.5 A and C).

After re-scaling and then normalizing¹³ with the basal side, the tendency that higher order junctions have a higher receptor intensity is still visible.

The Kruskal Wallis test rejects the null hypothesis and shows significant difference within the groups. Hence one can say that Podxl is inhomogeneously distributed, because it accumulates significantly more than the homogeneously distributed CAAX.

Follow up this idea, it is also tested, if the accumulation depends on the junction type. Again, the null hypothesis is H_0 : Higher order junctions have an equal Podxl concentration as lower order junctions.

After performing the Kruskal-Wallis test which reveals that Podxl accumulates, the Dunn test with Bonferroni correction reveals that that the (new) null-hypothesis has to be rejected as well for the 4 groups, except for the comparison between 3- and 4-cellular junctions (in some time steps). This means that a) Podxl is not homogeneously distributed in the organoid and b) Podxl enriches in higher order junctions more than in lower order junctions.

In the cases where 3- and 4-cellular junctions are different (Figure 4.5 D, at time steps without black cross), one can even say that the Podxl concentration increases with the junction order.

In the theory of lumen formation, the mESCs form a rosette before they open the lumen. The analysis of the location of Podxl enrichment is the indicator for lumen formation and is part of the next section.

4.7 Cells enrich Podocalyxin close to the geometrical center of the organoid, but still vary its exact position

After finding out the Podxl accumulates in higher order junction, it is now of interest to define the accumulation location of this receptor. The location is then the center of the rosette and the point where the lumen opens first (theoretically). To find this point, all Podxl within the organoid is analyzed cell-specific.

¹³In this step, a median value of zero for the basal side was avoided by deleting zero intensities from the measurements

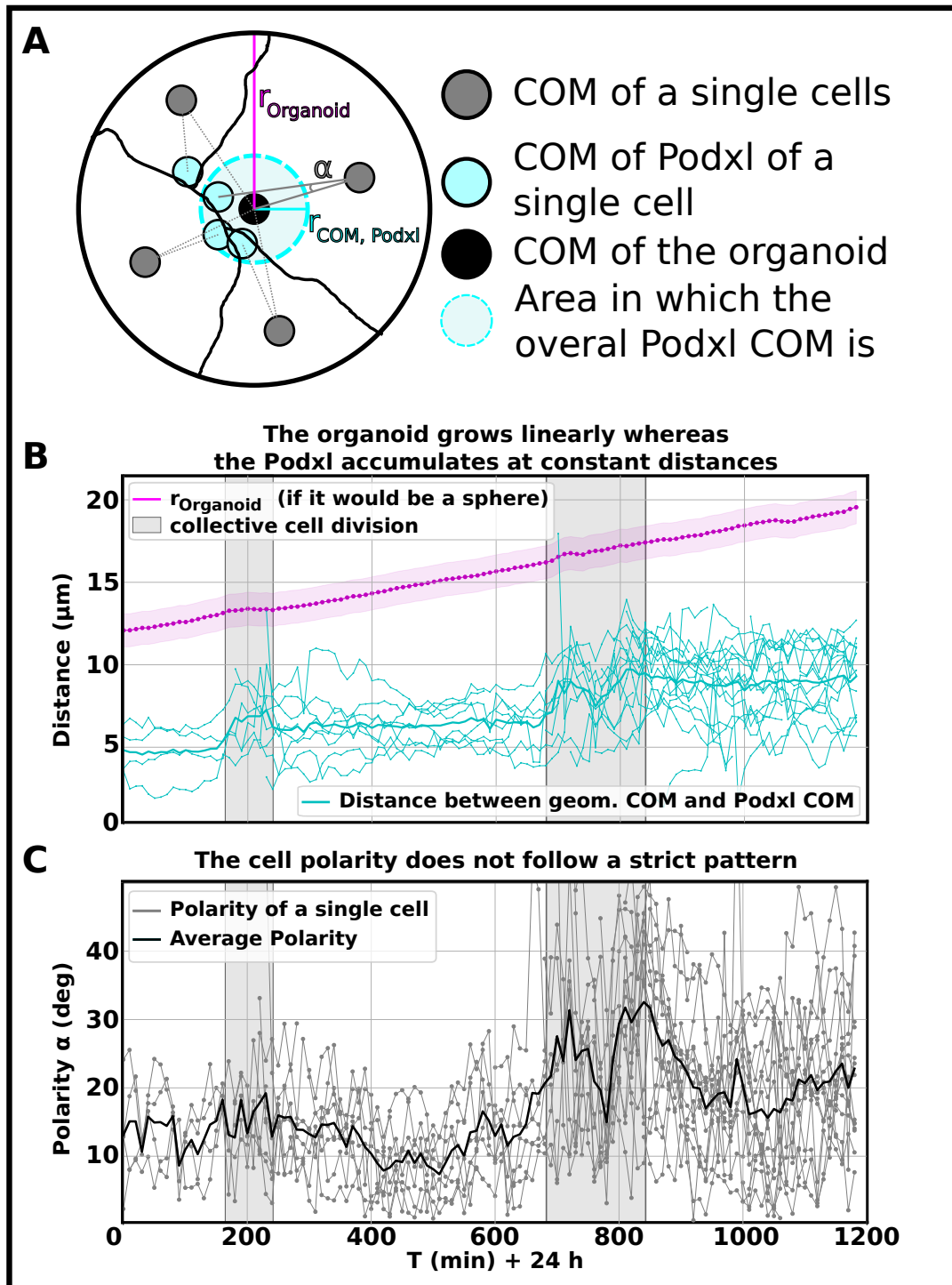


Figure 4.6: Podxl accumulates in the close distance around the geometrical COM of the organoid. A) 2D sketch of the 3D organoid with radius r_{Organoid} (magenta), consisting of 4 cells, with gray COMs and cyan Podxl COM. The angle (α) defines the polarity of cell-Podxl with respect to the organoid COM (black, compare C). The light cyan region with radius $r_{\text{COM}, \text{Podxl}}$ defines the distance in which the overall Podxl is accumulated (compare B). B) Radius of the organoid under spherical approximation in magenta. Distance between the Podxl COM and the geometrical COM cell wise (thin cyan line) and on average (thick cyan line). C) Polarity of the single cells (gray) and the average polarity (black). All data is plotted for the time of 24 hours plus $T = 0$ up to $T = 1200$ min.

Cells enrich Podocalyxin close to the geometrical center of the organoid, but still vary its exact position

Figure 4.6 A shows the measured parameters. In Figure 4.6 B one can see the COM of Podxl per cell in magenta (thin cyan lines) and their enrichment distance from the geometrical COM of the organoid. The average distance is plotted as a thick line. One can see that this distance is approximately constant for all 3 intervals and increases with every interval. As a comparison, the radius of the organoid¹⁴ is plotted in magenta. One can see that the cell divisions increase the distance from COM Podxl to the geometrical center, which is coupled with the increasing diameter of the accumulation point around the center. Also, the average distance is constant over these intervals, because this is the closest possible distance to the midpoint which is possible.

Taking a look at the cell polarization (α in Figure 4.6 C), one can see that the complete system is dynamic. Every cell polarity is able to change by several degrees, which describes the flexibility in the system. It means that the single cell Podxl COMs can vary flexibly, especially during cell divisions, but in general (Figure 4.6 B), they are always accumulating as close as possible to the geometrical COM.

Due to the knowledge that Podxl is important for lumen formation (Bryant, 2010; Ferrari, 2008), it makes sense that the average distance is stable within a certain range. Due to the fact that the cell just starts to differentiate it can be expected, that fluctuations in the position of the apical membrane are happening. This influences the polarization because Podxl is attached to the membrane. This effect can not be seen in MDCK organoids but in mESC organoids. It is a kind of unstable stability.

¹⁴Here the radius is calculated from the organoid volume under the assumption that the organoid is a sphere.

5 Discussion

In this thesis, the aim was to develop a quantitative image analysis pipeline for time-lapse microscopy to understand cell-interface self-organization during the process of organoid lumenogenesis. Software for 4D confocal image quantification, based on instance segmentation of cell boundaries is presented. This software allows getting insight into the development of 3D organoids, based on quantifiable physical parameters at the single cell level. This method was applied on 2-channel light-sheet microscopy data of self-organizing mouse embryonic stem cells and revealed for the first time the evolution of cell interfaces coupled to polarity protein distribution over the course of epiblast organoid formation.

Software for automated quantification of segmented 4D mESC data

The described software splits up into 2 parts. Part one is the improvement of already segmented data, followed by lineage tracing. Part two is the quantification of biological parameters. Within the improvement step of segmented data, the software uses information about the system (e.g. maximum number of cells or minimum volume of a cell compared to the average cell volume) and time information to connect 3D segmented data with each other in time to reach the best possible 4D segmentation results. The overall accuracy of the output is still limited by the accuracy of the segmentation methods on which it is based. These methods are the 3D U-Net architecture (Cicek, 2016), followed by GASP (Bailoni, 2019), and in post-processing steps also the seeded-WS method (Neubert, 2014). Even though 3D U-Nets are state-of-the-art border prediction networks, they struggle with the correct segmentation of a lumen in the membrane images. This is not surprising, because (a) the network does not know about the lumen, because it was never trained on it, and (b) even an experimenter can not discriminate the cell-lumen boundaries since the lumen of epiblast organoids is filled with membrane. In the future, one could define the lumen as an independent object which is classified by high receptor and high membrane concentration. For this, the code is already written, but not implemented into the workflow yet.

Overall, the software improves existing work to a new level and can be used confidently to quantify 4D cell development. This serves as a strong basis for performing morphological and receptor distribution measurements.

Morphological measurements indicate that cells proliferate with different rates

Performing morphological measurements based on the cell segmentation and 3D reconstruction revealed that cells grow in volume with an average rate of $(2.60 \pm 0.86) \mu\text{m}^3/\text{min}$

and in area with an average rate of $(0.88 \pm 0.71) \mu\text{m}^3/\text{min}$. growth rates are independent of the cell cycle up to the X cell stage. It would be interesting to see whether the growth rates change in later timepoints of development when there are more cells in the system and more space competition. Analyzing more organoids could reveal a difference in growth rates between volume and surface area and how the cell regulates its aspect ratios during the formation of an organoid rosette.

Receptor expression seems to tremendously increase, triggered by the exit from the pluripotent state

The measurements of the receptor expression at the single cell level indicate that the receptor expression is up-regulated once the cells are removed from pluripotency and placed in the extracellular matrix to differentiate. This makes sense since the receptor Podxl is a structural protein of the apical membrane and the cells are differentiated from stem cells to epithelial cells to create a lumen (Shahbazi, 2017). Hence the receptor has to be produced in time and in a huge amount, to reach high concentrations. With the help of single cell tracking, it is now possible to verify this for single cell development of mESC organoids. The preliminary results here would show that the concentration compared to the pluripotent state is then transported to the membrane and influence the cell interface interactions as previously reported (Klinkert, 2016; Bryant, 2014; Bodak, 2017; Cirera-Salinas, 2017).

Homogeneous membrane protein increases step-wise with the junction order

Analyzing only the cell interfaces revealed that homogeneously distributed membrane component signal (mNG-CAAX) indeed behaves as one would expect: it is significantly shown that a 2-fold junction has double amount of membrane as a 1-fold junction. Also, 3 and 4 fold junctions consist of 3 and 4 fold more membrane.

During the different cell cycles, this behavior varies and shows overexpression of membrane along 2 and 3 cellular junctions. It looks like the cell is collecting the membrane protein CAAX in these junction types until a certain concentration level is reached. This could be interpreted as the folding of the membrane resulting in the increased signal. After this maximum concentration, the CAAX concentration splits up into the different junction types in a way that the expected concentration per junction is reached. Splitting up into different junction types could mean that junctions are folded for so long, that two 2Js are so close together that they end up in a 3J or the same for 3Js and 4Js.

Apical membrane receptor Podxl inhomogeneously accumulates more in higher order junctions than in lower order junctions

Testing the concentration of Podxl along the cell interfaces revealed two things. First of all, it is shown that Podxl distributes inhomogeneously along the surface (compared

with CAAX). Secondly, it is shown that the concentration of Podxl increases additionally with the junction order.

This makes sense with the background knowledge that Podxl initializes the lumen formation and the knowledge that mESC forms a rosette before the lumen is initiated (Bryant 2014; Bedzhov 2014). So most of the receptor is transported to the center of the organoid and accumulates there at a high concentration. This high concentration of the anti-adhesive receptor Podxl leads then due to repulsive membrane interaction to lumen creation.

Considering the increasing concentrations and inhomogeneity, one can define acting forces on the receptor. Concentration gradients lead to a flux (λ), driven by a force (f). Fluxes are changes of thermodynamic variables ($\lambda = \frac{\delta c}{\delta t}$). The corresponding thermodynamic force is the change of the Free Energy (F) of the system with respect to the concentration $f = \frac{\delta F}{\delta c}$. This force from Podxl should be neglectable with respect to the forces, which the cell with its cytoskeleton can apply. So the cell can actively control the position of Podxl when it binds Podxl internally to the cytoskeleton.

Receptor accumulates with dynamic stability close to the geometrical COM

The second last step of lumenogenesis is the formation of a rosette, after which the lumen starts to open. After identifying, that higher order junctions contain the highest amounts of Podxl and with the knowledge that Podxl is necessary for lumen opening, the rosette center was tracked. Podxl accumulates stable in a certain ring around the geometrical COM. Nevertheless, it is still able to flow to different regions.

The measurement at the moment only considers the Podxl COM. One could make the measurement of the distance more accurate by using only concentrations which belong to 3J or 4J or one could just track the junctions itself. Only taking the single cell Podxl COMs into account can lead to imprecise results, when a cell has multiple Podxl accumulation points.

With a diameter threshold of the "high-intensity ring" around the COM, one could define lumen initiation in the future. With a defined lumen, one can then train the neural network again, so that it classifies the lumen by its own.

6 Conclusion

Previous papers and the results and discussion of this thesis indicate a way to describe lumogenesis in mESC organoids. These processes are formed by evolution and are not unique in mouse cells, so ideas can be applied to any kind of cells and processes.

Overall I can imagine that the lumogenesis within the development of mESCs looks like this:

Stem cells proliferate fast and start to reach the pluripotent exit (Bodak, 2017; Cirera-Salinas, 2017). After reaching this state, the cells start to differentiate. This is coupled to an increased Podxl production (Figure 4.3). The receptor is a system that can receive and transduce signals and helps the cell to detect contact sides. The cell could then have the aim to bring contact sides (so basically high receptor concentrations) close together, by folding the membrane (membrane folding could be visible in Figure 4.4 B, during the second interval). Due to the folding of the membrane, 3-cellular junctions come closer together and can form a 4J. This is connected to an increase of Podxl concentration (in Figure 3.6 B and D, the not different 3-4 junctions split up to distinguishable 3J and 4J, whereas the 4J has a higher concentration of receptor). From previous studies (Bedzhov, 2014) and from polarization measurements (Figure 4.6), it is then known that the rosette forms, where the Podxl is mostly located close to the geometrical COM. By then taking a look at the embryo development (Figure 4.1), one can see the offspring of the lumen. This lumen would then also have the highest possible amount of membrane for building the apical plasma membrane, similar to the MDCK cells (Bryant, 2010).

The general principle of building a lumen is an evolutionary stable process. That means that it is happening in a robust way in every organism of the species and it happens because it is the most efficient way without bottlenecks. The most efficient is connected to the most energy minimization pathway. This pathway could be a geometrical surface minimization based on the self-organization of the cell adhesion interfaces. Hence the basic principle could be included in other (model) species as well. Finally, a better understanding of tissue formation would bring uncountable advances in biological engineering and human health. It allows to improve regenerative medicine and to discover the origin of developmental diseases.

All these speculations are based on cell and cell interface quantifications, which are now automated, reliable, objective, and repeatable¹⁵ for everyone.

¹⁵For access to the software and data, please ask the lab head Alf Honigmann (TU Dresden, 2022) or Eric Schmidt (Eric_Schmidt_99@gmx.de)

Bibliography

- [1] Yara Alcheikh. *Lumen Formation of Mouse Embryonic Stem Cell Epiblast-Like Cysts in vitro*. Ph.D, TU Dresden, Dresden, February 2022.
- [2] Alberto Bailoni, Constantin Pape, Nathan Hütsch, Steffen Wolf, Thorsten Beier, Anna Kreshuk, and Fred A. Hamprecht. GASP, a generalized framework for agglomerative clustering of signed graphs and its application to Instance Segmentation. 2019. Publisher: arXiv Version Number: 2.
- [3] Ivan Bedzhov and Magdalena Zernicka-Goetz. Self-Organizing Properties of Mouse Pluripotent Cells Initiate Morphogenesis upon Implantation. *Cell*, 156(5):1032–1044, February 2014.
- [4] Serge Beucher. Use of watersheds in contour detection. Technical report, September 1979.
- [5] Maxime Bodak, Daniel Cirera-Salinas, Jian Yu, Richard P. Ngondo, and Constance Ciaudo. *Dicer*, a new regulator of pluripotency exit and LINE-1 elements in mouse embryonic stem cells. *FEBS Open Bio*, 7(2):204–220, February 2017.
- [6] David M. Bryant, Anirban Datta, Alejo E. Rodríguez-Fraticelli, Johan Peränen, Fernando Martín-Belmonte, and Keith E. Mostov. A molecular network for de novo generation of the apical surface and lumen. *Nature Cell Biology*, 12(11):1035–1045, November 2010.
- [7] David M. Bryant, Julie Roignot, Anirban Datta, Arend W. Overeem, Minji Kim, Wei Yu, Xiao Peng, Dennis J. Eastburn, Andrew J. Ewald, Zena Werb, and Keith E. Mostov. A Molecular Switch for the Orientation of Epithelial Cell Polarization. *Developmental Cell*, 31(2):171–187, October 2014.
- [8] Özgün Çiçek, Ahmed Abdulkadir, Soeren S. Lienkamp, Thomas Brox, and Olaf Ronneberger. 3D U-Net: Learning Dense Volumetric Segmentation from Sparse Annotation. Technical Report arXiv:1606.06650, arXiv, June 2016. arXiv:1606.06650 [cs] type: article.

- [9] Daniel Cirera-Salinas, Jian Yu, Maxime Bodak, Richard P. Ngondo, Kristina M. Herbert, and Constance Ciaudo. Noncanonical function of DGCR8 controls mESC exit from pluripotency. *Journal of Cell Biology*, 216(2):355–366, February 2017.
- [10] Regis Doyonnas, David B. Kershaw, Christian Duhme, Helen Merkens, Shierley Chelliah, Thomas Graf, and Kelly M. McNagny. Anuria, Omphalocele, and Perinatal Lethality in Mice Lacking the Cd34-Related Protein Podocalyxin. *Journal of Experimental Medicine*, 194(1):13–28, July 2001.
- [11] Paul Ducheyne, David W Grainger, Kevin E Healy, Dietmar W Hutmacher, and C. J Kirkpatrick. *Comprehensive biomaterials II*. 2017. OCLC: 988770643.
- [12] Aldo Ferrari, Alexey Veligodskiy, Ulrich Berge, Miriam S. Lucas, and Ruth Kroschewski. ROCK-mediated contractility, tight junctions and channels contribute to the conversion of a preapical patch into apical surface during isochoric lumen initiation. *Journal of Cell Science*, 121(21):3649–3663, November 2008.
- [13] Scott F. Gilbert, Teri Jo Mauch, and Gary C. Schoenwolf. Developmental Biology. Sixth Edition. By Scott F. Gilbert. *American Journal of Medical Genetics*, 99(2):170–171, March 2001.
- [14] Jan Huisken, Jim Swoger, Filippo Del Bene, Joachim Wittbrodt, and Ernst H. K. Stelzer. Optical Sectioning Deep Inside Live Embryos by Selective Plane Illumination Microscopy. *Science*, 305(5686):1007–1009, August 2004.
- [15] Anuradha Kar, Manuel Petit, Yassin Refahi, Guillaume Cerutti, Christophe Godin, and Jan Traas. Benchmarking of deep learning algorithms for 3D instance segmentation of confocal image datasets. *PLOS Computational Biology*, 18(4):e1009879, April 2022.
- [16] Yung Su Kim, Rui Fan, Ludmila Kremer, Nannette Kuempel-Rink, Karina Mildner, Dagmar Zeuschner, Liesbeth Hekking, Martin Stehling, and Ivan Bedzhov. Deciphering epiblast lumenogenesis reveals proamniotic cavity control of embryo growth and patterning. *Science Advances*, 7(11):eabe1640, March 2021.
- [17] Kerstin Klinkert, Murielle Rocancourt, Anne Houdusse, and Arnaud Echard. Rab35 GTPase couples cell division with initiation of epithelial apico-basal polarity and lumen opening. *Nature Communications*, 7(1):11166, September 2016.
- [18] Manan Lalit, Pavel Tomancak, and Florian Jug. EmbedSeg: Embedding-based Instance Segmentation for Biomedical Microscopy Data. *Medical Image Analysis*, 81:102523, October 2022.

0 Bibliography

- [19] Ngoc Le Tran, Yao Wang, and Guiying Nie. Podocalyxin in Normal Tissue and Epithelial Cancer. *Cancers*, 13(12):2863, June 2021.
- [20] Denise K. Marciano. A holey pursuit: lumen formation in the developing kidney. *Pediatric Nephrology*, 32(1):7–20, January 2017.
- [21] Cécilie Martin-Lemaitre, Yara Alcheikh, Ronald Naumann, and Alf Honigmann. Optimization of mouse embryonic stem cell culture for organoid and chimeric mice production. preprint, Cell Biology, March 2020.
- [22] Andrea Meinhardt, Dominic Eberle, Akira Tazaki, Adrian Ranga, Marco Niesche, Michaela Wilsch-Bräuninger, Agnieszka Stec, Gabriele Schackert, Matthias Lutolf, and Elly M. Tanaka. 3D Reconstitution of the Patterned Neural Tube from Embryonic Stem Cells. *Stem Cell Reports*, 3(6):987–999, December 2014.
- [23] Kelly McNagny, Michael R., Marcia L., Erin J., Kimberly Snyder, Jane Cipollone, Michelle Turvey, Poh C., Shaun McColl, and Calvin D. Podocalyxin in the Diagnosis and Treatment of Cancer. In Ravinder Mohan, editor, *Advances in Cancer Management*. InTech, January 2012.
- [24] Peer Neubert and Peter Protzel. Compact Watershed and Preemptive SLIC: On Improving Trade-offs of Superpixel Segmentation Algorithms. In *2014 22nd International Conference on Pattern Recognition*, pages 996–1001, Stockholm, Sweden, August 2014. IEEE.
- [25] Olaf Ronneberger, Philipp Fischer, and Thomas Brox. U-Net: Convolutional Networks for Biomedical Image Segmentation. In Nassir Navab, Joachim Hornegger, William M. Wells, and Alejandro F. Frangi, editors, *Medical Image Computing and Computer-Assisted Intervention – MICCAI 2015*, volume 9351, pages 234–241. Springer International Publishing, Cham, 2015. Series Title: Lecture Notes in Computer Science.
- [26] Johannes Schindelin, Ignacio Arganda-Carreras, Erwin Frise, Verena Kaynig, Mark Longair, Tobias Pietzsch, Stephan Preibisch, Curtis Rueden, Stephan Saalfeld, Benjamin Schmid, Jean-Yves Tinevez, Daniel James White, Volker Hartenstein, Kevin Eliceiri, Pavel Tomancak, and Albert Cardona. Fiji: an open-source platform for biological-image analysis. *Nature Methods*, 9(7):676–682, July 2012.
- [27] Uwe Schmidt, Martin Weigert, Coleman Broaddus, and Gene Myers. Cell Detection with Star-convex Polygons. volume 11071, pages 265–273. 2018. arXiv:1806.03535 [cs].

- [28] Marta N. Shahbazi, Antonio Scialdone, Natalia Skorupska, Antonia Weberling, Gaelle Recher, Meng Zhu, Agnieszka Jedrusik, Liani G. Devito, Laila Noli, Iain C. Macaulay, Christa Buecker, Yakoub Khalaf, Dusko Ilic, Thierry Voet, John C. Marioni, and Magdalena Zernicka-Goetz. Pluripotent state transitions coordinate morphogenesis in mouse and human embryos. *Nature*, 552(7684):239–243, December 2017.
- [29] Sara Sigurbjörnsdóttir, Renjith Mathew, and Maria Leptin. Molecular mechanisms of de novo lumen formation. *Nature Reviews Molecular Cell Biology*, 15(10):665–676, October 2014.
- [30] Austin G. Smith, John K. Heath, Deborah D. Donaldson, Gordon G. Wong, J. Moreau, Mark Stahl, and David Rogers. Inhibition of pluripotential embryonic stem cell differentiation by purified polypeptides. *Nature*, 336(6200):688–690, December 1988.
- [31] Nicholas Sofroniew, Talley Lambert, Kira Evans, Juan Nunez-Iglesias, Grzegorz Bokota, Philip Winston, Gonzalo Peña-Castellanos, Kevin Yamauchi, Matthias Bussonnier, Draga Doncila Pop, Ahmet Can Solak, Ziyang Liu, Pam Wadhwa, Alister Burt, Genevieve Buckley, Andrew Sweet, Lukasz Migas, Volker Hilsenstein, Lorenzo Gaifas, Jordão Bragantini, Jaime Rodríguez-Guerra, Hector Muñoz, Jeremy Freeman, Peter Boone, Alan Lowe, Christoph Gohlke, Loic Royer, Andrea PIERRÉ, Hagai Har-Gil, and Abigail McGovern. napari: a multi-dimensional image viewer for Python, May 2022.
- [32] Carsen Stringer, Tim Wang, Michalis Michaelos, and Marius Pachitariu. Cellpose: a generalist algorithm for cellular segmentation. *Nature Methods*, 18(1):100–106, January 2021.
- [33] C. Sullivan and Alexander Kaszynski. PyVista: 3D plotting and mesh analysis through a streamlined interface for the Visualization Toolkit (VTK). *Journal of Open Source Software*, 4(37):1450, May 2019.
- [34] R. Lindsay Williams, Douglas J. Hilton, Shirley Pease, Tracy A. Willson, Colin L. Stewart, David P. Gearing, Erwin F. Wagner, Donald Metcalf, Nicos A. Nicola, and Nicholas M. Gough. Myeloid leukaemia inhibitory factor maintains the developmental potential of embryonic stem cells. *Nature*, 336(6200):684–687, December 1988.
- [35] Adrian Wolny, Lorenzo Cerrone, Athul Vijayan, Rachele Tofanelli, Amaya Vilches Barro, Marion Louveaux, Christian Wenzl, Sören Strauss, David Wilson-Sánchez, Rena Lymbouridou, Susanne S Steigleder, Constantin Pape, Alberto Bailoni, Salva

0 Bibliography

Duran-Nebreda, George W Bassel, Jan U Lohmann, Miltos Tsiantis, Fred A Hamprecht, Kay Schneitz, Alexis Maizel, and Anna Kreshuk. Accurate and versatile 3D segmentation of plant tissues at cellular resolution. *eLife*, 9:e57613, July 2020.

Declaration of Research Integrity and Good Scientific Practice

I hereby certify that I have authored this Master's Thesis entitled "Quantification of cell interface dynamics during mouse epiblast organoid formation by using SPIM imaging and segmentation analysis" and without undue assistance from third parties. No other than the resources and references indicated in this thesis have been used. I have marked both literal and accordingly adopted quotations as such. There were no additional persons involved in the spiritual preparation of the present thesis. I am aware that violations of this declaration may lead to subsequent withdrawal of the degree.

Dresden, 23.08.2022

Eric Schmidt